PHYSICAL REVIEW A **98**, 023428 (2018)

Discrete-resonance-resonance transitions induced by two laser pulses with an ultrashort time delay: A formal analytic solution and quantitative applications

Yannis Komninos,[*] Theodoros Mercouris,[†] and Cleanthes A. Nicolaides[‡]
Theoretical and Physical Chemistry Institute, National Hellenic Research Foundation,
48 Vasileos Constantinou Avenue, Athens 11635, Greece

(Received 16 April 2018; published 30 August 2018)

The paper presents a theory that solves analytically the time-dependent three-level problem of the scheme discrete $|0\rangle \xrightarrow[\text{as pulse } \omega_1]{\text{weak}}$ resonance $|1\rangle \xrightarrow[\text{fs pulse } \omega_2]{\text{moderately strong}}$ resonance $|2\rangle$, where $|0\rangle$ is a discrete state, and $|1\rangle$ and $|2\rangle$ are energy-normalized resonance states. The attosecond and femtosecond pulses with central frequencies ω_1 and ω_2 ($\omega_1 \gg \omega_2$) act with ultrashort time delay, t_D. The formalism leads to *analytic* expressions for photoelectron emission probabilities, $P_i(E,t)$, $i = 1, 2$, in the energy region of the two resonance states, whose calculation in terms of *N*-electron matrix elements and external control parameters can be carried out economically for any such three-level system. The problem is first solved analytically, within the rotating wave approximation, for the case where the femtosecond pulse is rectangular. The weak attosecond pulse can have any temporal shape. The final solution for two pulses with arbitrary shape (Gaussian in our case) is then achieved by fitting numerically the shape of the femtosecond pulse to a sum of rectangular pulses. The formulas for $P_i(E,t)$ involve, among other things, the Fano *discrete-resonance* asymmetry parameter q, and the *resonance-resonance* asymmetry parameter Q, defined by us in previous work. They also involve the *complex energy poles* of the two resonances, a result which accounts for the whole contribution of the open channels of energy-normalized scattering states into which they decay. The theory is applied to the calculation from first principles, using compact *state-specific* discrete and resonance wave functions, of observable aspects of the time-resolved dynamics associated with the processes He $1s^2\ {}^1S \rightarrow (2s2p)\ {}^1P^o \leftrightarrow (2p^2)\ {}^1D$. Calculations show that the $(2p^2)\ {}^1D$ resonance is 0.295 eV (4200 nm) below the energy of $(2s2p)\ {}^1P^o$, (60.15 eV), and its width is 0.067 eV. For the transition $1s^2\ {}^1S \rightarrow (2s2p)\ {}^1P^o$, the full width at half maximum (FWHM) of the Gaussian pulse is 160 as. The few-cycle midinfrared pulse coupling the resonance states is also Gaussian, whose duration is varied in the range of a few decades of femtoseconds. Its intensity is in the range 5×10^{10}–5×10^{11} W/cm^2. The external control parameters are the intensity and the FWHM of the femtosecond pulse, as well as the t_D. For a given value of t_D, the FWHM of the second pulse is a crucial control parameter. The results include the time-resolved formation of either the $(2s2p)\ {}^1P^o$ or the $(2p^2)\ {}^1D$ resonance, while they are coupled with each other. For the $(2s2p)\ {}^1P^o$ state, comparison is made with the case where the time-dependent buildup of its asymmetric profile, excited from $1s^2\ {}^1S$ by the same attosecond pulse, is calculated in the absence of coupling to another resonance. The result is in harmony with that of our earlier work on this problem. For the $(2p^2)\ {}^1D$ resonance excited from $(2s2p)\ {}^1P^o$, the time-resolved buildup of its profile does not develop into an asymmetric peak due to the fact that Q has the very large value of ≈ -1300. Instead, it finishes as an Autler-Townes doublet.

DOI: 10.1103/PhysRevA.98.023428

I. INTRODUCTION

We consider the known problem of an atom interacting with two ultrashort pulses, one with attosecond (as) duration and central frequency ω_1 and the other with few-cycle femtosecond (fs) duration and central frequency ω_2 ($\omega_1 \gg \omega_2$). The external control parameters are the time delay t_D, with which the two pulses act (positive, zero, or negative), the peak intensities of the two fields, and the duration of each pulse. Given that, in the realistic case, the temporal shapes of the pulses are best represented by a Gaussian function, the duration is defined here by the value of its full width at half maximum (FWHM).

From the theoretical point of view, the solution of problems with real atoms and molecules arising from such ultrashort interactions rests on the possibility of determining reliably, and of using efficaciously in the appropriate theoretical context, the *many-electron* time-dependent wave function $\Psi(t)$, containing the relevant physical information. The $\Psi(t)$ satisfies the *many-electron time-dependent Schrödinger equation* (METDSE), where the total Hamiltonian $\boldsymbol{H}(t)$ has the form $\boldsymbol{H}(t) = \mathbf{H}_{\text{atom}} + \boldsymbol{V}_1(\omega_1, t) + \boldsymbol{V}_2(\omega_2, t + t_D)$. The present paper discusses a practical solution of the METDSE with such a $\boldsymbol{H}(t)$, for the quantitative understanding of aspects of the physics that takes place under special conditions of an atomic spectrum, in connection to the characteristics of the two pulses.

A. The problem

In earlier proposals and results regarding possible applications of the then emerging prospects of spectroscopy

---

[*] ykomn@eie.gr
[†] thmerc@eie.gr
[‡] caan@eie.gr

2469-9926/2018/98(2)/023428(17)

using attosecond pulses, we singled out as a fruitful area of investigation the time-dependent coherent excitation (by one or two ultrafast pulses) and decay of strongly correlated doubly excited states (DESs) and of inner-hole excited states, caused by effects of evolving superpositions and of ultrafast electron rearrangements inside the continuum of scattering states [1–4]. The wave functions of such states are a superposition of localized (square-integrable) and of asymptotically scattering components. If this superposition is described accurately, then their intrinsic properties, namely the energy position in the continuum and the energy width, as well as probabilities (or rates) of transitions involving such states, can be determined reliably.

As the prototypical case for testing such ideas, we developed theory and carried out calculations which revealed quantitatively the time-resolved evolution of the low-lying $^1P^o$ DESs of helium, pulse-excited from the $1s^2\ ^1S$ or the $1s2s\ ^1S$ metastable state. Indeed, the prediction for the time-resolved formation of the photoionization profile for He $1s^2\ ^1S \rightarrow (2s2p)^1P^o$ at 60.15 eV [3] was recently verified experimentally by Kaldun, Blättermann *et al.* [5,6], via a measurement technique capable of attosecond time resolution.

In this paper, we first report on a formalism for the solution of a problem involving the time-dependent coupling by ultrafast pulses of resonance states. Then, by choosing an experimentally convenient case from the helium spectrum that is again based on the attosecond-pulsed transition He $1s^2\ ^1S \rightarrow (2s2p)^1P^o$ (see below), we report the quantitative findings from *ab initio* calculations that have employed state-specific wave functions.

Specifically, this formalism leads to *analytic* expressions for time-dependent probabilities of photoelectron emission in the region of resonances, as a function of parameters of ultrashort pulses and of the time delay in their application, for the following *discrete-resonance-resonance* excitation-coupling scheme, scheme (A):

$$\text{discrete}|0\rangle \xrightarrow[\text{as pulse } \omega_1]{\text{weak}} \text{resonance}|1\rangle \xrightarrow[\text{fs pulse } \omega_2]{\text{moderately strong}} \text{resonance}|2\rangle.$$

ω_1 and ω_2 are equal to the corresponding differences between the state energies, although small detunings may be present. The energy of $|2\rangle$ may be above or below that of $|1\rangle$.

As a paradigm for the computational application of the theory for scheme (A), we chose the two-color process in scheme (B):

$$\text{He}1s^2 \xrightarrow[60.15\,\text{eV}]{160\text{ - as Gaussian pulse}} (2s2p)^1P^o \xrightarrow[0.295\,\text{eV}]{\text{fs Gaussian pulse}} (2p^2)^1D.$$

The parentheses on the configurational label signify the fact that this is the main configuration in the superposition of the localized and asymptotic components of the resonance state.

The He $(2p^2)^1D$ resonance lies at about 0.295 eV ($\lambda \approx 4200$ nm) below the $(2s2p)\ ^1P^o$ in the continuous spectrum [7]. Its width is about 0.067 eV [7] and the energy for its ionization to the He^+2p threshold is 5.5 eV. The duration (i.e., the FWHM) of the weak attosecond Gaussian pulse is chosen to be 160 as, the value that was used recently in the experiment of Kaldun *et al.* [5]. The intensity of the few-cycle, femtosecond midinfrared (MIR) Gaussian laser pulse is in the experimentally practical range of 5×10^{10}–$5\times10^{11}\,\text{W/cm}^2$, which, as it turned out, is sufficient for allowing the demonstration of distinguishable phenomena as a function of external control parameters. The time delay t_D ranges from positive to negative femtosecond values, including the region of zero.

We point out that the energetics do not allow ionization by the mid-IR pulse of either the $(2s2p)\ ^1P^o$ or the $(2p^2)^1D$ state. This fact, in conjunction with the choice of low intensities for the MIR laser, eliminates the need to consider additional effects caused by field-induced ionization.

Scheme (A) involving the He $(2s2p)\ ^1P^o$ resonance, has been examined before, experimentally as well as theoretically, with respect to coupling to the $(2s^2)\ ^1S$ resonance below it (≈540-nm fs pulse), or to the $(2p^2)\ ^1S$ resonance above it, (≈800-nm fs pulse) [8–17]. The discussions in [8–17] explain their methods and results. Here, it suffices to note that the emphasis has been on the exploration of the changes that occur for the asymmetric photoionization profile of the process He $1s^2\ ^1S \rightarrow (2s2p)^1P^o$, when $(2s2p)\ ^1P^o$ is coupled resonantly to $(2s^2)\ ^1S$ or $(2p^2)\ ^1S$, as a function of the field strength and of t_D.

The published theoretical work has produced probabilities of photoelectron emission as well as of photoabsorption in the energy region of the $(2s2p)\ ^1P^o$ resonance. As regards the types of calculations, these may be separated into two categories, distinguished by the way they tackle the problem of determining the physically relevant $\Psi(t)$. In the first category, $\Psi(t)$ is first written as a superposition of two-electron wave functions with time-dependent coefficients. The two-electron wave functions are constructed in terms of a common basis set, and represent states of both the discrete and the continuous spectrum. The calculation solves numerically the coupled equations into which the two-electron TDSE is transformed upon substitution of this $\Psi(t)$ [13,15,17]. Even for helium, the size of the calculations that are based on such an expansion is considerable, given that, for a thorough study of the phenomena, the external control parameters of the two pulses have to be varied systematically. For example, in the first such calculation for helium, involving the coupling of the $(2s2p)\ ^1P^o$ and $(2p^2)\ ^1S$ resonances by an intense 800-nm laser with duration of 42 fs, Tarana and Greene [13] commented briefly on the increased computational requirements in such studies, concluding that, "*there is no method which enables a routine theoretical calculation of the photoabsorption spectra in the presence of a strong dressing-laser pulse*" (page 1 of [13]).

In the second category [10–12], the expansion of $\Psi(t)$ is reduced to a time-dependent three-level (TD3L) model, employed by Madsen *et al.* [18] for the calculation of ion yields in a problem of earlier interest, where the pulses were assumed to be long. As with all models of a few resonantly interacting states, such a reduction ignores the possible mixing of states and of scattering continua in higher order. Yet a number of complexities concerning the calculation of the reduced $\Psi(t)$ describing scheme (A) remain. In the approach of [10–12], approximations that neglect certain couplings, including the "*adiabatic elimination of continua*" were made. For example, Chu and Lin [12] note that, "*with our first approximation* [i.e., the neglect of the cross dipole matrix elements between the localized and the asymptotic components of the two resonances], *q cannot be defined for the* $|b_2\rangle$-$|E_2\rangle$ *resonance*" (page 2 of [12]). ($|b_2\rangle$ is the localized component and $|E_2\rangle$ is the scattering component of the second resonance.) Using such simplifications, Chu and Lin [10–12] solved the resulting system of coupled equations *numerically*, for the $1s^2\ {}^1S \rightarrow (2s2p)^1P^o \leftrightarrow (2s^2)^1S$ and the $1s^2\ {}^1S \rightarrow (2s2p)^1P^o \leftrightarrow (2p^2)^1S$ ultrafast excitation-coupling schemes, and presented a series of results and conclusions for different values of external parameters.

Finally, we note that effects on the photoexcitation profile in the energy region of an autoionizing state that is coupled to another resonance by a relatively strong field were computed and observed in the laboratory for doubly excited states of the two-electron helium [19] and of the pseudo-two-electron magnesium [20], in frameworks that are applicable to long pulses (ac field). The corresponding formalisms and possibilities of analysis are less versatile, since they do not depend on the *ab initio* solution of the METDSE where the matter-field interaction involves ultrashort pulses. In treatments such as those of [19,20], even in principle no information can be obtained on time scales of attoseconds or a few femtoseconds.

B. Introductory comments on the present approach

The present study is also based on the reduction of the full expansion to a TD3L model corresponding to scheme (A), but without the simplifying approximations that were made previously. In addition, the theory achieves *analytic* expressions for the photoelectron emission probability. These refer not only to the vicinity of resonance $|1\rangle$ but also to the vicinity of $|2\rangle$. Once the *N*-electron wave functions and corresponding matrix elements are available, the calculations using these expressions are managed easily, and can be repeated for different values of the external parameters with great economy of time, even on small computers.

The reduction of the exact problem of having to solve the METDSE with the electronic Hamiltonian $\boldsymbol{H}(t)$ in terms of an "infinite" number of coupled equations involving the stationary states of the discrete and the continuous spectrum to that described by a TD3L system is an approximation whose degree of validity is linked to the quantity of interest, to the choice of the atomic (molecular) spectrum and of the field parameters, and to the method used to calculate $\Psi(t)$ in the restricted space.

Obviously, if rigor and accuracy are the goals, it cannot be *a priori* justified for the case where the field of the pulse coupling the two resonance states becomes very strong. (The phrase "very strong" depends on each case and its borderline is quantifiable only after quantitative calculations.) This is because once an autoionizing state $|1\rangle$ has been prepared by a weak excitation from a discrete state, $|0\rangle$, its interaction with a dc or an ac field, or with an ultrashort pulse of radiation, perturbs the wave function to a degree that depends on the spectrum, on the electronic structures, and on the characteristics of the interaction. A thus perturbed wave function has consequences for the properties of the resonance energy position and width, as well as for transition processes in which it is involved, such as the photoabsorption profile, which depends on the matrix elements of the total Hamiltonian and on the field parameters. Indeed, if the strength of the field coupling the two resonances becomes strong, it is inevitable that the field-atom interaction will cause extra effects due to the field-induced mixing of other quasidiscrete (resonance) or discrete states and of additional scattering channels contributing in higher order. For example, some time ago, the implementation of a time-independent *nonperturbative* formalism with state-specific wave functions showed quantitatively how the energies and the rates of decay, including induced radiative autoionization, of DESs that are coupled to other DESs via ac or dc electric [21,22] or magnetic [23] fields, vary as a function of frequency or intensity, while many scattering continua contribute in higher order. Effects such as those discussed in [21–23] (e.g., variation of stability via the field-induced crossing of DESs of thresholds in the multichannel continuum) can, in principle, also be present in the context of ultrashort pulsed interactions.

In our work on the time-resolved photoionization in the region of the He $(2s2p)\ {}^1P^o$ resonance state [3], which is the first step of scheme (B), the problem was solved from two very different approaches. In the first, $\Psi(t)$ was calculated by solving nonperturbatively the METDSE in terms of the *state-specific expansion approach* (SSEA) [24]. In the SSEA, the number of the coupled equations is normally in the thousands or even in the few hundreds of thousands (the overwhelming number coming from the energy-normalized scattering functions representing the continuous spectrum), and contain energies and *bound-bound*, *bound-free*, and *free-free* matrix elements [25]. The solution, $\Psi_{SSEA}(t)$, is transparent and valid for weak as well as for strong fields. However, its calculation is, in general, computationally demanding and time consuming. Hence, given the nature of the problem in [3], we also proposed and implemented an *analytic*, time-dependent two-level approach, which is valid for weak ultrashort pulses and which allows very economic calculations of the *discrete-to-resonance* state time-dependent excitation probability. The agreement between the results of the two approaches for weak pulses was excellent (Fig. 2 of [3]), demonstrating that the theory leading to the analytic expression and to its implementation is not restricted to descriptive phenomenology, and that its numerical results, obtained using state-specific wave functions for discrete and resonance states, are reliable.

The pulse-dependent analytic formula of [3] was derived by choosing the stationary representation of the resonance state according to the energy-normalized superposition of localized with scattering components given by the Fano formalism [26]. It is a product of three energy-dependent factors:

(1) A Lorentzian distribution function.

(2) A spectral-asymmetry function modifying the Lorentzian to an asymmetric Fano shape.

(3) A function which depends on the pulse and is associated with the time dependence of the process.

The probability that the photoelectron remains temporally trapped for time intervals of the order of the lifetime of the autoionizing state is obtained by subtracting from the product the value which it acquires on the complex resonance energy, $E_r - i\Gamma$ (Γ is the half width).

Similar features, albeit incorporated into more complex formulas, are found in the formalism of the present paper for the solution of problems that are described by scheme (A). Indeed, one of the special results of the theory for both the two-level and the three-level systems is the appearance in the analytic expressions of *complex energy poles* of the resonances, which take into account in a condensed way the contribution of the whole energy continuum into which each resonance state is embedded.

The formulas derived in the next section for scheme (A) give the photoelectron emission time-dependent probability not only for scattering energies in the vicinity of $|1\rangle$, but also for energies in the vicinity of the second resonance, $|2\rangle$. The formalism and its underlying concepts are such that the possible applications are not restricted to two-electron systems. Extension to resonances embedded in multichannel continua is feasible.

The main features of the formalism are the following:

(1) The formulas for the two channels, $|1\rangle$ and $|2\rangle$, derived in the following sections, are expressed as products of the three types of factors discussed above in connection to our two-level model for discrete to resonance state transitions, albeit with the time-dependent factor now being a much more complicated function. Thus, the transparency of the simpler two-level case has been retained, while accounting in a comprehensive way for the contributions of the main couplings. The derivation of these formulas is achieved based on two legitimate assumptions: First, the rotating wave approximation (RWA) is good. Second, the effect on the observables of the extremely small coupling between the open-channel components of the resonance wave functions is negligible.

(2) Both pulses can have any of the commonly used shapes, including the realistic Gaussian one, with a duration in the range of attoseconds or femtoseconds. For example, in the application to scheme (B) presented in this paper, (Sec. IV), both pulses have a Gaussian shape. The intensities are within experimentally controllable ranges. The coupled equations for the time-dependent complex expansion coefficients of the stationary states describing the scheme (A) are solved analytically.

(3) As in our previous work, the theory for scheme (A) is constructed by using the stationary description of energy-normalized resonance states, in the superposition of localized and scattering components which was formulated by Fano [26].

The results of the theory are applicable to both $|1\rangle$ and $|2\rangle$ resonances and the corresponding continua. The solutions produce the photoelectron probability distributions in the two open channels. The scope of the theory for this TD3L model does not include the *ab initio* calculation of possible minute effects of spontaneous radiative emission (widths can be added for, say, the fast radiative decay of inner-hole states of heavy atoms) or possible effects of energy shifts and ionization widths induced by very strong fields. If needed, the formalism can be expanded in order to approximate their contributions in terms of additional parameters.

(4) The analytic formulas involve, among other things, the use of two computable quantities that have to do with the two steps of (A): One quantity is Fano's q, corresponding to the *discrete-resonance* transition [26]. The second quantity is Q, corresponding to the *resonance-resonance* transition [27]. Its utility for the proper interpretation of the details in resonance-resonance radiative transitions was demonstrated in [28], in connection to the measurements and interpretation reported in [29] concerning spectra of Rydberg series of resonances.

(5) Last but not least, the theory is not restricted to the use of parameters that are either assumed or are taken from published work, nor to cases of two-electron systems only. Instead, its formalism can be implemented in terms of computable N-electron matrix elements involving the states of interest. The *state- and property-specific* approach which is used in our case for the calculation of the required wave functions is reviewed in [30,31]. Examples of calculations of such wave functions and properties of helium DESs can be found in [1–3,7,27,32]. Their principal characteristic is the introduction and implementation of methods that combine advanced theory of decaying states and of multichannel scattering theory with electronic structure theory which is based on the solution of *state-specific* Hartree-Fock (HF) or multiconfigurational HF (MCHF) equations and on the additional calculation of the corresponding systematic corrections that are due to property-specific electron correlations [30,31].

The theory is presented in Sec. II. Because the derivation is necessarily long, the essential features are summarized in Sec. III. Section IV contains the results of the first application of the theory, which has to do with the calculation of observable aspects of the time-resolved electron dynamics associated with process (B).

II. PHOTOELECTRON EMISSION PROBABILITIES IN THE TD3L SYSTEM WITH TWO ULTRASHORT PULSES AND RESONANCE-RESONANCE COUPLING

The mathematical development which follows is divided into six subsections A–F. In subsection A, the problem is formulated in terms of a time-dependent superposition that includes the localized and the asymptotically scattering *components* of the two states. The sought after amplitude of photoelectron emission probability for each channel, $A_{iE}(t)$, $i = 1, 2$, is defined in terms of the time-dependent mixing coefficients, which satisfy a system of integrodifferential equations. Subsection B presents certain physically important functions of transition matrix elements entering the calculation and the justifiable approximations which are made in order to render the system of equations solvable analytically. In subsection C, a simple transformation of the mixing coefficients allows the energy integrals to be evaluated by contour integration. The system of integrodifferential equations is transformed into a system of ordinary differential ones. In subsection D, the latter system is solved analytically, assuming a rectangular temporal shape for the second pulse. The case where the second pulse has an arbitrary shape is solved semianalytically, by fitting its shape to a sum of rectangular pulses. Finally, the formal results are presented in subsections E and F.

A. Formal expression for the photoelectron emission probability

The time-dependent wave function of the atomic system is expanded in terms of the eigenstates as ($\hbar = 1$)

$$|\Psi(t)\rangle = |\Psi_g\rangle e^{-iE_gt}c_g(t) + \sum_{i=1}^{2}\int dE|\Psi_{iE}\rangle e^{-iEt}c_{iE}(t). \quad (1)$$

The electronic Hamiltonian is thus diagonal in the continuous part of the spectrum for each angular momentum. Ψ_g is the ground state (or initial discrete state) of angular momentum L, and $i = 1, 2$ denotes the $L \pm 1$ and $L \pm 2$ or L states respectively. In the stationary representation on the real energy axis, the resonance state wave function is written in terms of its localized, ϕ_i, and scattering, $|u_{iE}\rangle$, components as [26]

$$|\Psi_{iE}\rangle = \alpha_i(E)\left[|\phi_i\rangle + P\int dE'|u_{iE'}\rangle\frac{1}{E-E'}V_{iE'} + |u_{iE}\rangle\frac{E-E_i}{V_{iE}}\right]. \tag{2}$$

In our work, the zero-order scattering orbitals entering $|u_{iE}\rangle$ are obtained in the term-dependent fixed-core HF approximation, so as to eliminate *intrachannel* coupling.

The symbol P stands for principal-value integration. Also,

$$V_{iE} = \langle\phi_i|\mathbf{H}_{\rm atom}|u_{iE}\rangle \quad\text{and}\quad \alpha_i(E) = \frac{V_{iE}}{\sqrt{(E-E_i)^2+\Gamma_i^2}} \tag{3a}$$

for $i = 1, 2$, where $\Gamma_{iE} = \pi V_{iE}^2$ is the half width of the resonance. As usual, it is assumed to be equal to its value at the resonance energy E_i, where

$$E_i = \langle\phi_i|\mathbf{H}_{\rm atom}|\phi_i\rangle + P\int dE' V_{iE'}\frac{1}{E-E'}V_{iE'}. \tag{3b}$$

The factor $\alpha_i(E)$, whose square is the Lorentzian distribution, will play an important role in the formalism that follows.

The quantity of interest is the probability $P_i(E,t) \equiv |A_{iE}(t)|^2$ for $i = 1, 2$, to observe an outgoing electron into one of the ionization channels with $L \pm 1$ and $L \pm 2$ or L angular momentum. In order for it to be accurate for times when the autoionizing states have not been depleted, we subtract the survival amplitude from the total one:

$$A_{iE}(t) = \langle\Psi_{iE} \mid \Psi(t)\rangle - \alpha_i(E)\langle\phi_i \mid \Psi(t)\rangle. \tag{4}$$

The $\Psi(t)$ satisfies the METDSE,

$$i\frac{\partial}{\partial t}\Psi(t) = \left[\mathbf{H}_{\rm atom} + \sum_{j=1}^{2}\boldsymbol{V}_{(j)}(\omega_j,t)\right]\Psi(t), \tag{5a}$$

where

$$\boldsymbol{V}_{(j)}(\omega_j,t) = zF_jg_j(t)\sin(\omega_jt-\varphi_j) \tag{5b}$$

represents the perturbation by two laser pulses with $\omega_1 \approx E_1 - E_g$ and $\omega_2 \approx E_2 - E_1$. The two linearly polarized pulses act with a time delay t_D. For the symmetries of the problem, the only nonzero dipole matrix elements are

$$D_{g,1E} = \langle\Psi_g|z|\Psi_{1E}\rangle \quad\text{and}\quad D_{1E,2\bar{E}} = \langle\Psi_{1E}|z|\Psi_{2\bar{E}}\rangle. \tag{5c}$$

Substituting Eq. (1) into Eq. (5a) and taking matrix elements leads to the system of equations for the time-dependent coefficients:

$$ie^{-iE_gt}\dot{c}_g = F_1g_1(t)\sin(\omega_1t-\varphi_1)\int dE'\,D_{g,1E'}e^{-iE't}c_{1E'}, \tag{6a}$$

$$ie^{-iEt}\dot{c}_{1E} = F_1g_1(t)\sin(\omega_1t-\varphi_1)D_{1E,g}e^{-iE_gt}c_g + F_2g_2(t)\sin(\omega_2t-\varphi_2)\int dE'D_{1E,2E'}e^{-iE't}c_{2E'}, \tag{6b}$$

$$ie^{-iEt}\dot{c}_{2E} = F_2g_2(t)\sin(\omega_2t-\varphi_2)\int dE'D_{2E,1E'}e^{-iE't}c_{1E'}, \tag{6c}$$

where the dot symbolizes the time derivative.

In terms of the coefficients, Eq. (4) becomes

$$A_{iE}(t) = e^{-iEt}c_{iE}(t) - \alpha_i(E)\int dE'\alpha_i(E')e^{-iE't}c_{iE'}(t). \tag{7}$$

Therefore, it is necessary to obtain the coefficients $c_{iE}(t)$ from the integrodifferential Eqs. (6). To this end, we must have the explicit expressions for the dipole matrix elements $D_{g,1E}$ and $D_{1E,2\bar{E}}$. The fulfillment of this task leads naturally to the introduction of the *spectral-asymmetry* functions.

B. Spectral-asymmetry functions: The emergence of Fano-type complex generalized quantities (parameters)

Substituting the wave function (2) into the definitions (5c) we obtain

$$D_{1E,g} = \alpha_1(E)b_{1E} \equiv \alpha_1(E)\left[d_{1g}(E) + \frac{E-E_1}{V_{1E}}d_{1E,g}\right] \tag{8a}$$

and

$$D_{1E,2\bar{E}} \approx \alpha_1(E)\alpha_2(\bar{E})b_{1E,2\bar{E}} \equiv \alpha_1(E)\alpha_2(\bar{E})\left[d_{1,2}(E,\bar{E}) + \frac{E-E_1}{V_{1E}}d_{1E,2} + \frac{\bar{E}-E_2}{V_{2\bar{E}}}d_{2\bar{E},1}\right]. \tag{8b}$$

In deriving (8b), we have ignored the contribution of the extremely small dipole matrix elements $d_{1E,2E'} = \langle u_{1E}|z|u_{2E'}\rangle$ involving the unperturbed continua.

These expressions define the *spectral-asymmetry* functions b_{1E} and $b_{1E,2\bar{E}}$. The quantities $d_{1g}(E)$ and $d_{1,2}(E,\bar{E})$ include the contributions from the integral of the second term in Eq. (2). The full expression for the formula (8b), which includes the free-free transitions, can be found in Ref. [27].

The function b_{1E} for the discrete to resonance transition derived from Eq. (8a) is expressed in terms of the asymmetry parameter $q = d_{1g}/\pi V_{1E_1}d_{1E_1,g}$, where the matrix elements are considered constant in the vicinity of the resonance:

$$b_{1E}{=}\pi V_{1E_1}d_{1E_1,g}\left[q + \frac{E-E_1}{\Gamma_1}\right] \tag{9a}$$

When the square of this function multiplies the Lorentzian distribution, it produces the Fano result for the spectral profile.

Similarly, we express the spectral-asymmetry function $b_{1E,2\bar{E}}$ for the resonance to resonance transition derived from Eq. (8b),

$$b_{1E,2\bar{E}} \approx \left(\pi V_{1E_1}d_{1E_1,2} + \pi V_{2E_2}d_{2E_2,1}\right) \times\left[Q + \frac{E-E_1}{\Gamma_1}\gamma_1 + \frac{\bar{E}-E_2}{\Gamma_2}\gamma_2\right], \tag{9b}$$

in terms of a generalized Fano-type Q parameter,

$$Q = d_{12}/\big(\pi V_{1E_1} d_{1E_1,2} + \pi V_{2E_2} d_{2E_2,1}\big), \tag{9c}$$

which results from the treatment of *free-free* transitions [27].

The definition of the quantities γ_1, γ_2 and Q results easily from Eq. (8b), e.g., $\gamma_1 = \pi V_{1E_1} d_{1E_1,2}/(\pi V_{1E_1} d_{1E_1,2} + \pi V_{2E_2} d_{2E_2,1})$, etc. The quantities γ_i are a kind of branching ratio. According to their definition, $\gamma_1 + \gamma_2 = 1$. Again, matrix elements appear in these formulas with their values on the corresponding resonance. Note that, since the basis functions are real, the matrix elements of Eqs. (9) are also real, and $b_{1E,2\bar{E}} = b_{2\bar{E},1E}$.

As will be shown, it is not the function (9b) itself which appears in the spectra but its values on one of the two poles, Eqs. (10b) and (10c) below. For the sake of completeness, we also give explicitly the constants (10a) and (10d) which also appear in the formulas,

$$b_{1z_1} = \pi V_{1E_1} d_{1E_1,g}(q - i), \tag{10a}$$

$$b_{1z_1,2E} = \big(\pi V_{1E_1} d_{1E_1,2} + \pi V_{2E_2} d_{2E_2,1}\big) \times \left[Q - i\gamma_1 + \frac{E - E_2}{\Gamma_2}\gamma_2\right], \tag{10b}$$

$$b_{1E,2z_2} = \big(\pi V_{1E_1} d_{1E_1,2} + \pi V_{2E_2} d_{2E_2,1}\big) \times \left[Q - i\gamma_2 + \frac{E - E_1}{\Gamma_1}\gamma_1\right], \tag{10c}$$

$$b_{1z_1,2z_2} = \big(\pi V_{1E_1} d_{1E_1,2} + \pi V_{2E_2} d_{2E_2,1}\big)(Q - i). \tag{10d}$$

The quantity $b_{1z_1,2E}$ of Eq. (10b) is linked to the transition to the second channel. Its role for this channel is the same as that of b_{1E} of Eq. (9a) for the transition from the ground state to the first channel, i.e., it contributes to the asymmetry of the resonance to resonance transition, Eq. (46) below, which would otherwise be symmetric due to the Lorentzian $\alpha_2^2(E)$. However, as seen from Eq. (10b), this transition involves the complex generalized parameter $(Q - i\gamma_1)/\gamma_2$.

The same role is fulfilled by the quantity $b_{1E,2z_2}$ in Eq. (38) below, for the term describing the transition to the first channel from the population accumulated at the second one, with the complex generalized parameter $(Q - i\gamma_2)/\gamma_1$. On the other hand, the first term in Eq. (38) describing the discrete to resonance transition contains the Fano asymmetry function b_{1E}.

The resonance profiles are generally asymmetric and the asymmetry is controlled by the *inverse* of the asymmetry parameter. A large asymmetry parameter results in an essentially symmetric curve—the imaginary part contributes to the symmetric part. In the case of the *resonance to resonance* transition, the quantity Q is typically large for the normally considered doubly excited states, as the dipole matrix elements from the localized parts to the continua are small. Hence, the asymmetry becomes noticeable only in the case of a small dipole matrix element connecting the localized parts.

C. Transition to a system of differential equations

The system of the integrodifferential Eqs. (6) will now be reduced to a manageable system of differential equations. Substituting the matrix elements (8a) and (8b) in the system of Eqs. (6) we obtain

$$\dot{c}_g = -iF_1 e^{iE_g t} g_1(t)\sin(\omega_1 t - \varphi_1)\int dE'\,\alpha_1(E')\,b_{1E'}e^{-iE't}c_{1E'}, \tag{11a}$$

$$\dot{c}_{1E} = -i\alpha_1(E)F_1 e^{-i(E_g-E)t} g_1(t)\sin(\omega_1 t - \varphi_1)\,b_{1E}c_g - i\alpha_1(E)F_2 e^{iEt} g_2(t)\sin(\omega_2 t - \varphi_2)\int dE' b_{1E,2E'}\alpha_2(E')e^{-iE't}c_{2E'}, \tag{11b}$$

$$\dot{c}_{2\bar{E}} = -i\alpha_2(\bar{E})F_2 e^{i\bar{E}t} g_2(t)\sin(\omega_2 t - \varphi_2)\int dE' b_{2\bar{E},1E'}\alpha_1(E')e^{-iE't}c_{1E'}, \tag{11c}$$

where b_{1E} and $b_{1E,2\bar{E}}$ are defined in Eqs. (8a) and (8b). From inspection of Eqs. (11), it follows that the coefficients c_{iE} are proportional to the quantities $\alpha_i(E)$.

Accordingly, we transform to the more convenient variables C_{iE},

$$c_{1E} = \alpha_1(E)\,C_{1E}, \quad c_{2E} = \alpha_2(E)\,C_{2E}, \tag{12}$$

which satisfy the equations (the time dependence is indicated explicitly)

$$\dot{c}_g(t) = -iF_1 e^{iE_g t} g_1(t)\sin(\omega_1 t - \varphi_1)\int dE'\,\alpha_1^2(E')\,b_{1E'}e^{-iE't}C_{1E'}(t), \tag{13a}$$

$$\dot{C}_{1E}(t) = -iF_1 e^{-i(E_g-E)t} g_1(t)\sin(\omega_1 t - \varphi_1)\,b_{1E}c_g(t) - iF_2 e^{iEt} g_2(t)\sin(\omega_2 t - \varphi_2)\int dE' b_{1E,2E'}\alpha_2^2(E')e^{-iE't}C_{2E'}(t), \tag{13b}$$

$$\dot{C}_{2\bar{E}}(t) = -iF_2 e^{i\bar{E}t} g_2(t)\sin(\omega_2 t - \varphi_2)\int dE' b_{2\bar{E},1E'}\alpha_1^2(E')e^{-iE't}C_{1E'}(t). \tag{13c}$$

Consequently, the energy integrations can be performed noting that, from the definition (3a),

$$\alpha_i^2(E) = \frac{1}{\pi}\frac{\Gamma_i}{(E-E_i)^2+\Gamma_i^2}. \tag{14}$$

The Lorentzian distribution $\alpha_i^2(E)$ can be written as a function with two poles in the complex plane:

$$\alpha_i^2(E) = \frac{1}{2\pi i}\left[\frac{1}{E-z_i^*} - \frac{1}{E-z_i}\right],$$
$$z_i = E_i - i\Gamma_i \tag{15}$$

Performing in Eqs. (13) the contour integration in the lower half plane, traversed in the clockwise sense, the first term of (15) gives zero while the second results in

$$\frac{1}{2\pi}\int dE\,\frac{e^{-iEt}}{E-z_i}F(E) = -ie^{-iz_it}F(z_i) \tag{16}$$

for any analytic function $F(z)$. In addition, the assumption of the RWA leads to the following system of differential equations:

$$\dot{c}_g(t) = -\tfrac{1}{2}e^{-i\varphi_1}F_1g_1(t)\,b_{1z_1}e^{i(E_g+\omega_1-z_1)t}C_{1z_1}(t), \tag{17a}$$

$$\dot{C}_{1E}(t) = \tfrac{1}{2}e^{i\varphi_1}F_1g_1(t)b_{1E}e^{i(E-E_g-\omega_1)t}\,c_g(t)$$
$$-\tfrac{1}{2}e^{-i\varphi_2}F_2g_2(t)b_{1E,2z_2}e^{i(E+\omega_2-z_2)t}C_{2z_2}(t), \tag{17b}$$

$$\dot{C}_{2\bar{E}}(t) = \tfrac{1}{2}e^{i\varphi_2}F_2g_2(t)b_{2\bar{E},1z_1}e^{i(\bar{E}-\omega_2-z_1)t}C_{1z_1}(t). \tag{17c}$$

This is a remarkable result, as the contribution of an uncountable infinity of terms is replaced by the contribution from the two poles.

Equations (17) for the coefficients of the eigenstates present in the expansion (1) [via the transformation of Eq. (12)] constitute the basis of the present theory. It is for this reason that the derivation has been given in reasonable detail.

The same procedure, applied to Eq. (7), results in the form

$$A_{iE}(t) = \alpha_i(E)\big[e^{-iEt}C_{iE}(t) - e^{-iz_it}C_{iz_i}(t)\big], \quad i = 1, 2. \tag{18}$$

Consequently, the solution of Eqs. (17) determines the photoelectron emission amplitudes.

In order to perform the time integration in Eqs. (17), the functional dependence on time of the coefficients $C_{1z_1}(t)$ and $C_{2z_2}(t)$, i.e., the value of $C_{iE}(t)$ at the pole z_i, is needed. These satisfy the equations

$$\dot{c}_g(t) = -\tfrac{1}{2}e^{-i\varphi_1}F_1g_1(t)\,b_{1z_1}e^{i(E_g+\omega_1-z_1)t}C_{1z_1}(t), \tag{19a}$$

$$\dot{C}_{1z_1}(t) = \tfrac{1}{2}e^{i\varphi_1}F_1g_1(t)b_{1z_1}e^{i(z_1-E_g-\omega_1)t}\,c_g(t)$$
$$-\tfrac{1}{2}e^{-i\varphi_2}F_2g_2(t)b_{1z_1,2z_2}e^{i(z_1+\omega_2-z_2)t}C_{2z_2}(t), \tag{19b}$$

$$\dot{C}_{2z_2}(t) = \tfrac{1}{2}e^{i\varphi_2}F_2g_2(t)b_{2z_2,1z_1}e^{i(z_2-\omega_2-z_1)t}C_{1z_1}(t). \tag{19c}$$

As is evident from the derivation of Eq. (18) from Eqs. (7) and (4), the quantities $e^{-iz_i}C_{iz_i}(t)$ are the coefficients of the localized parts of the resonances. Similar equations appear in [9–12,18], where the total wave function is not expanded in terms of the exact resonance eigenfunctions, but in terms of the zero-order basis functions $|\phi_i\rangle$ and $|u_{iE}\rangle$, and the coupled equations are solved numerically. The relation between the two sets of coefficients have been given in our Ref. [3] [see Eqs. (17) where, however, the e^{-iEt} factor has not been written explicitly].

Because of the assumption of a weak and short initial pulse, we take $c_g \approx 1$. Consequently, Eq. (17a) is decoupled from the system of Eqs. (17), and Eq. (17b) now has an inhomogeneous term. This term takes into account the action of the first pulse. For its envelope we choose a Gaussian function, $g_1(t) = e^{-(t-t_a)^2/2\sigma_a^2}$, centered at $t = t_a$. These considerations apply to the system of Eqs. (19) as well.

We approximate the envelope of the second pulse,g_2, by a rectangular function,

$$g_2(t) \approx St(t-t_0) - St(t-t_1). \tag{20}$$

$St(t)$ is the step function which is unity if the argument is positive and zero otherwise. This pulse is centered at about t_b, where $t_b = (t_1 - t_0)/2$.

For times $t < t_0$, when $g_2(t)$ is zero, Eq. (17b) can be immediately integrated to give C_{1E}. Defining

$$G(E,t) = \int_{-\infty}^{t} dt' e^{i(E-E_g-\omega_1)t'}g_1(t')$$
$$\equiv \int_{-\infty}^{t} dt' e^{i(E-E_1+\Delta\omega_1)t'}g_1(t') \tag{21}$$

we obtain

$$C_{1E}(t) = \tfrac{1}{2}F_1e^{i\varphi_1}b_{1E}G(E,t), \quad t \leqslant t_0. \tag{22}$$

C_{1z_1} is the value of Eq. (22) at $E = z_1$ while $C_{2\bar{E}}$ and C_{2z_2} are equal to zero. Substituting this form into Eq. (18), we obtain the solution for a single pulse, given in [3].

In the following section, we shall derive the analytic solution of Eqs. (19b) and (19c) for $t_0 < t < t_1$ when $g_2(t)$ is nonzero. We shall then generalize the results to the case where $g_2(t)$ is approximated by a sum of rectangular pulses, each defined in a time interval $t_i < t < t_{i+1}$, with different heights g_i. In this way, any realistic pulse shape can be approximated reliably by using a large enough number of intervals $[t_i, t_{i+1}]$. In the applications of the present work, we have chosen Gaussian temporal shapes.

In subsections E and F we shall use these solutions to integrate the basic Eqs. (17b) and (17c). The analytic forms provide significant insight and facility of computation. The reader who is interested only in the final result may avoid the lengthy derivation by going straight to the final formulas (36) and (42).

D. Analytic solution when the second pulse is rectangular and extension to the case of an arbitrary temporal shape.

We now proceed to solve the system of Eqs. (19b) and (19c) when the second pulse is a rectangle. We start by defining real and complex quantities for detuning:

$$\Delta\omega_1 = E_1 - E_g - \omega_1,$$
$$a_1 = z_1 - E_g - \omega_1 = \Delta\omega_1 - i\Gamma_1, \tag{23a}$$
$$\Delta\omega_2 = E_2 - E_1 - \omega_2,$$
$$a = z_2 - z_1 - \omega_2 = \Delta\omega_2 + i(\Gamma_1 - \Gamma_2). \tag{23b}$$

The exponentials appearing in the system are expressed in terms of the complex detunings. We also define the coupling parameter,

$$\Lambda = g_2 F_2 b_{1z_1,2z_2}. \tag{24}$$

Although g_2 is presently equal to unity, it is included in the definition for later purposes. It is important to realize that the imaginary part of $b_{1z_1,2z_2}$ results from the part of the transition (8b) connecting the localized component to the scattering one. Through the complex detuning (23b) and the complex coupling parameter (24), a complex Rabi frequency is defined as

$$\lambda = \sqrt{a^2 + \Lambda^2} \quad (\text{complex Rabi frequency}). \tag{25}$$

The quantity λ represents the frequency of oscillations between the two decaying states. Note that, according to definition (23b), the complex detuning remains nonzero even when its real part $\Delta\omega_2$ is zero. Therefore, λ is never equal to the coupling parameter Λ. The possibility of $\lambda = \Lambda$ holds only for discrete states.

The method of solving the system of Eqs. (19b) and (19c) is described in Appendix A. The solution is written in terms of the integrals,

$$\begin{aligned} G^{(1)}(w^{\pm}, t) &= \int_{t_0}^{t} dt' e^{ia_1 t'} e^{i(a\mp\lambda)t'/2} g_1(t') \\ &\equiv \int_{t_0}^{t} dt' e^{iw^{\pm}t'} g_1(t') \end{aligned} \quad , \quad t < t_1, \tag{26a}$$

where

$$w^{\pm} = a_1 + (a \mp \lambda)/2. \tag{26b}$$

In the case where the envelope function is a Gaussian, the analytic expression of the $G^{(1)}$ integrals is given in terms of the error function (see Appendix B). We obtain

$$C_{1z_1}(t) = \frac{1}{2} e^{i\varphi_1} F_1 b_{1z_1} \left[\frac{(a+\lambda)}{2\lambda} e^{-i(a-\lambda)t/2} (c^{+} + G^{(1)}(w^{+}, t)) - \frac{(a-\lambda)}{2\lambda} e^{-i(a+\lambda)t/2} (c^{-} + G^{(1)}(w^{-}, t)) \right], \tag{27a}$$

$$C_{2z_2}(t) = -\frac{i}{2} e^{i\varphi_1} F_1 b_{1z_1} e^{i\varphi_2} F_2 b_{1z_1,2z_2} g_2(t) \left[\frac{1}{2\lambda} e^{i(a+\lambda)t/2} (c^{+} + G^{(1)}(w^{+}, t)) - \frac{1}{2\lambda} e^{i(a-\lambda)t/2} (c^{-} + G^{(1)}(w^{-}, t)) \right]. \tag{27b}$$

The values of the coefficients c^{+} and c^{-} are computed by the matching of the solutions Eqs. (22) and (27) at the time $t = t_0$. This is done below for the generalized form of g_2 which is a sum of rectangular functions as the one introduced in Eq. (20), namely,

$$g_2(t) \approx \sum_{i=1}^{n} g_i [St(t - t_{i-1}) - St(t - t_i)], \tag{28}$$

with n being an odd number. For the central rectangle, $N = \frac{1}{2}(n+1)$, we put $g_N = 1$, while for $i \neq N$, $g_i < 1$. If we require the function to be symmetrical, then $g_{N+k} = g_{N-k}$. The values of g_i can be made to fit any envelope function—a Gaussian $e^{-(t-t_b)^2/2\sigma_b^2}$ in our case -, centered at $t = t_b$. This is done in a systematic way in Appendix C where the chosen function is represented in a series of successively refined partitioning of time, until convergence is secured. The chosen parameters are $k = 10$ and $p = 2$, corresponding to $2^k - 1$ rectangles of width $2p\sigma_b/2^{k-1}$, which approximate the Gaussian in the interval $[t_b - 2p\sigma\ ,\ t_b + 2p\sigma]$.

The coefficients $C_{1z_1}(t)$ and $C_{2z_2}(t)$ are given again by Eqs. (27) at each time interval $t_i \leqslant t \leqslant t_{i+1}$ in terms of the quantities $\Lambda_i = g_i F_2 b_{1z_1,2z_2}$, $\lambda_i = \sqrt{a^2 + \Lambda_i^2}$, $w_i^{\pm} = a_1 + (a \mp \lambda_i)/2$, and $G_i^{(1)}(w_i^{\pm}, t)$, the latter calculated for t_i as the lower bound. The constants c_i^{+} and c_i^{-} at each interval are determined from those of the interval at the left by the continuity conditions $C_{1z_1(i)}(t_{i-1}) = C_{1z_1(i-1)}(t_{i-1})$ and $C_{2z_2(i)}(t_{i-1}) = C_{2z_2(i-1)}(t_{i-1})$ where we have set $C_{1z_1(0)}(t) = \frac{1}{2} F_1 e^{i\varphi_1} G(z_1, t) b_{1z_1}$ and $C_{2z_2(0)}(t) = 0$ for values of time $t < t_0$. Defining $\bar{C}_{1z_1}$ and $\bar{C}_{2z_2}$ from the relations

$$\begin{aligned} &C_{1z_1}(t) = \tfrac{1}{2} e^{i\varphi_1} F_1 b_{1z_1} \bar{C}_{1z_1}(t) \quad \text{and} \\ &C_{2z_2}(t) = -i \tfrac{1}{2} e^{i\varphi_1} F_1 b_{1z_1} e^{i\varphi_2} F_2 b_{1z_1,2z_2} g_2(t) \bar{C}_{2z_2}(t), \end{aligned} \tag{29}$$

we obtain from Eqs. (27)

$$\begin{aligned} c_j^{+} = {} & e^{i(a-\lambda_j)t_{j-1}/2} \bar{C}_{1z_1(j-1)} - (a - \lambda_j) \\ & \times e^{-i(a+\lambda_j)t_{j-1}/2} \frac{g_{j-1}}{g_j} \bar{C}_{2z_2(j-1)}, \end{aligned} \tag{30a}$$

$$\begin{aligned} c_j^{-} = {} & e^{i(a+\lambda_j)t_{j-1}/2} \bar{C}_{1z_1(j-1)} - (a + \lambda_j) \\ & \times e^{-i(a-\lambda_j)t_{j-1}/2} \frac{g_{j-1}}{g_j} \bar{C}_{2z_2(j-1)}. \end{aligned} \tag{30b}$$

It follows from the above discussion and results that the Rabi frequency at each interval is different. Note that, as $\Lambda_1 \to 0$, at the start of the Gaussian pulse, $\lambda \to a$, $w^{+} \to a_1$, and $G^{(1)}(w^{+}, t) \to G(z_1, t) - G(z_1, t_0)$, and therefore $C_{1z_1(1)}(t) \to \frac{1}{2} F_1 e^{i\varphi_1} b_{1z_1} [G(z_1, t) - G(z_1, t_0)]$ and $C_{2z_2(1)}(t) \to 0$. At the end of the second pulse, C_{1z_1} and C_{2z_2} have attained constant values.

At this point, it is worth mentioning that one can relax the condition $c_g \approx 1$ for the coefficient of the ground state, by approximating the first pulse by a sum of rectangular functions, getting an analytic solution for the three-level problem. However, this approach would complicate significantly the semianalytic solution with no substantial gain for a weak initial pulse.

The coefficients $C_{1z_1}(t)$ and $C_{2z_2}(t)$ are now known. From them, the coefficients $C_{1E}(t)$ and $C_{2E}(t)$ can be computed for all energies. This is done in the next two subsections.

E. Analytic results for the first ionization channel

With the form of C_{2z_2} known, Eq. (17a) is integrated in the region $t_0 \leqslant t' < t$, with the restriction $t \leqslant t_1$, and an expression for the coefficient $C_{1E}(t)$ is obtained.

Assuming the RWA, one has

$$C_{1E}(t) = \frac{1}{2}e^{i\varphi_1}F_1 b_{1E}G(E,t) - \frac{1}{2}e^{-i\varphi_2}F_2 b_{1E,2z_2}\int_{t_0}^{t} dt' g_2(t')e^{i(E-z_2+\omega_2)t'}C_{2z_2}(t')$$
$$\equiv \frac{1}{2}e^{i\varphi_1}F_1 b_{1E}G(E,t) - \frac{1}{2}e^{-i\varphi_2}F_2 b_{1E,2z_2}\int_{t_0}^{t} dt' g_2(t')e^{i(E-z_1)t'}e^{-iat'}C_{2z_2}(t'). \tag{31}$$

Substituting $C_{2z_2}(t)$ from Eq. (27b), the integrals to be evaluated have the form

$$G^{(2)}(\zeta^{\pm}, w^{\pm}, t) = \int_{t_0}^{t} dt' g_2(t')e^{i(E-z_1)t'}e^{-i(a\mp\lambda)t'/2}[c^{\pm} + G^{(1)}(w^{\pm}, t')]$$
$$\equiv \int_{t_0}^{t} dt' e^{i\zeta^{\pm}t'}[c^{\pm} + G^{(1)}(w^{\pm}, t')], \quad t \leqslant t_1, \tag{32a}$$

where

$$\zeta^{\pm}(E) = E - z_1 + \frac{1}{2}(-a \pm \lambda) = E - E_1 + \frac{1}{2}(-\Delta\omega_2 \pm \mathrm{Re}\lambda) + \frac{i}{2}(\Gamma_1 + \Gamma_2 \pm \mathrm{Im}\lambda). \tag{32b}$$

Then

$$C_{1E}(t) = \frac{1}{2}e^{i\varphi_1}F_1 b_{1E}G(E,t) + \frac{i}{8\lambda}e^{i\varphi_1}F_1 b_{1z_1}F_2 b_{1E,2z_2}\Lambda[G^{(2)}(\zeta^{+}, w^{+}, t) - G^{(2)}(\zeta^{-}, w^{-}, t)]. \tag{33}$$

As it is shown in Appendix B, the integrals $G^{(2)}(\zeta^{\pm}, t)$ in Eqs. (32a) and (33) are expressed in terms of the integrals $G^{(1)}(w^{\pm}, t)$ and $G^{(1)}(w^{\pm} + \zeta^{\pm}, t)$.

Since $w^{\pm} + \zeta^{\pm} = E - E_1 + \Delta\omega_1$, the second integral is independent of the parameter λ, therefore the upper and the lower sign lead to the same result. It is equal to $G^{(1)}((E - E_1 + \Delta\omega_1), t) \equiv G(E,t) - G(E,t_0)$ [see Eq. (25)]. Defining

$$P_{1E}(t) = \frac{1}{4\lambda\zeta^{+}}e^{i\zeta^{+}t}[c^{+} + G^{(1)}(w^{+}, t)] - \frac{1}{4\lambda\zeta^{-}}e^{i\zeta^{-}t}[c^{-} + G^{(1)}(w^{-}, t)\,]$$
$$- \frac{1}{4\lambda\zeta^{+}}e^{i\zeta^{+}t_0}c^{+} + \frac{1}{4\lambda\zeta^{-}}e^{i\zeta^{-}t_0}c^{-} + \frac{1}{4\zeta^{+}\zeta^{-}}[G(E,t) - G(E,t_0)] \tag{34}$$

and substituting (B2) to Eq. (33), we obtain

$$C_{1E}(t) = \tfrac{1}{2}e^{i\varphi_1}F_1 b_{1E}G(E,t) + \tfrac{1}{2}e^{i\varphi_1}F_1 b_{1z_1}F_2 b_{1E,2z_2}\Lambda P_{1E}(t). \tag{35}$$

It is easy to check that in the limit $E \to z_1$, when $\zeta_{\pm} \to (-a \pm \lambda)/2$ from the definition (32b), Eq. (35) reduces to $C_{1z_1}(t)$ of Eq. (27a). Bringing together these results, we obtain the expression for the amplitude:

$$A_{1E}(t) = \alpha_1(E)\tfrac{1}{2}e^{i\varphi_1}F_1\big[e^{-iEt}b_{1E}G(E,t) + F_2^2 b_{1z_1}b_{1z_1,2z_2}$$
$$\times e^{-iEt}b_{1E,2z_2}P_{1E}(t) - e^{-iz_1t}b_{1z_1}\bar{C}_{1z_1}(t)\big], \tag{36}$$

where $\bar{C}_{1z_1}(t)$ is defined in Eq. (29). We observe that, in forming the probability $|A_{iE}(t)|^2$, the symmetric Lorentzian distribution $\alpha_1^2(E)$ is multiplied by a factor composed of three terms. The first term describes the effect of the first pulse in the absence of the second one. The last term is also present in this case, albeit modified. The spectral-asymmetry function b_{1E} is responsible for changing the Lorentzian to an asymmetric Fano spectral line and the time dependence is controlled by the integral $G(E,t)$ (see also [3]). In the presence of the second pulse, the amplitude is modified by the second term which contains the function $b_{1E,2z_2}$ and whose time dependence is controlled by the more complicated function $P_{1E}(t)$. Finally, we note that the second term of Eq. (36) is multiplied by the intensity F_2^2 of the second pulse.

Presently, the approximation by a single rectangular pulse, Eq. (20), is replaced by a summation of rectangular pulses, Eq. (28), and the integral in Eqs. (31)–(32b) is replaced by a sum of integrals

$$\sum_{i=1}^{m} g_i \int_{t_{i-1}}^{t} dt' e^{i(E-z_1)t'}e^{-iat'}C_{2z_2(i-1)}(t'), \quad t \leqslant t_m$$

For $t > t_n$, i.e., after the end of the last pulse, this function becomes a constant equal to its value at $t = t_n$.

F. Analytic results for the second ionization channel

In the same framework, Eq. (17b) is integrated in the region $t_0 \leqslant t' < t$, with the restriction $t \leqslant t_1$, and an expression for the coefficient $C_{2E}(t)$ is obtained:

$$C_{2E}(t) = \frac{1}{2}e^{i\varphi_2}F_2 b_{1z_1,2E}\int_{t_0}^{t} dt' g_2(t')e^{i(E-z_1-\omega_2)t'}C_{1z_1}(t')$$
$$\equiv \frac{1}{2}e^{i\varphi_2}F_2 b_{1z_1,2E}\int_{t_0}^{t} dt' g_2(t')e^{i(E-z_2)t'}e^{iat'}C_{1z_1}(t'). \tag{37}$$

Substituting $C_{1z_1}(t)$ from Eq. (27a), the integrals to be evaluated have the form

$$\begin{aligned} G^{(2)}(\xi^{\pm}, w^{\pm}, t) &= \int_{t_0}^{t} dt' g_2(t') e^{i(E-z_2)t'} e^{i(a\pm\lambda)t'/2}[c^{\pm} + G^{(1)}(w^{\pm}, t')] \\ &\equiv \int_{t_0}^{t} dt' e^{i\xi^{\pm}(E)t'}[c^{\pm} + G^{(1)}(w^{\pm}, t')], \quad t \leqslant t_1, \end{aligned} \tag{38a}$$

where

$$\xi^{\pm}(E) = E - z_2 + \frac{1}{2}(a \pm \lambda) = E - E_2 + \frac{1}{2}(\Delta\omega_2 \pm \mathrm{Re}\lambda) + \frac{i}{2}(\Gamma_1 + \Gamma_2 \pm \mathrm{Im}\lambda). \tag{38b}$$

Then,

$$C_{2E}(t) = \frac{1}{8\lambda} e^{i\varphi_1} F_1 b_{1z_1} e^{i\varphi_2} F_2 b_{1z_1,2E}[(a+\lambda)G^{(2)}(\xi^+, w^+, t) - (a-\lambda)G^{(2)}(\xi^-, w^-, t)]. \tag{39}$$

The $G^{(2)}$ integrals have the same form as Eq. (33). However, in this case they contain the characteristics of the second resonance. As in the previous section, the integrals $G^{(2)}(\xi^{\pm}, t)$ are expressed in terms of the integrals $G^{(1)}(w^{\pm}, t)$ and $G^{(1)}(w^{\pm} + \xi^{\pm}, t)$.

Since $w^{\pm} + \xi^{\pm} = E - E_2 + \Delta\omega_2 + \Delta\omega_1$, the second integral is independent of the parameter λ, therefore the upper and the lower sign lead to the same result. Using (B2) of Appendix B and defining

$$\begin{aligned} P_{2E}(t) = {} & \frac{a+\lambda}{4\lambda\xi^+} e^{i\xi^+ t}[c^+ + G^{(1)}(w^+, t)] - \frac{a-\lambda}{4\lambda\xi^-} e^{i\xi^- t}[c^- + G^{(1)}(w^-, t)] \\ & - \frac{a+\lambda}{4\lambda\xi^+} e^{i\xi^+ t_0} c^+ + \frac{a-\lambda}{4\lambda\xi^-} e^{i\xi^- t_0} c^- - \frac{1}{2\xi^+\xi^-}(E - z_2) G^{(1)}((E - E_2 + \Delta\omega_2 + \Delta\omega_1), t), \end{aligned} \tag{40}$$

we obtain

$$C_{2E}(t) = -\frac{i}{2} F_1 e^{i\varphi_1} b_{1z_1} e^{i\varphi_2} F_2 b_{1z_1,2E} P_{2E}(t). \tag{41}$$

It is easy to check that in the limit $E \to z_2$, when $\xi_{\pm} \to (a \pm \lambda)/2$ from the definition (40b), Eq. (42) reduces to $C_{2z_2}(t)$ of Eq. (27b). Bringing together the previous results, we obtain the expression for the amplitude:

$$A_{2E}(t) = -\frac{i}{2}\alpha_2(E) e^{i\varphi_1} F_1 b_{1z_1} e^{i\varphi_2} F_2 \big[e^{-iEt} b_{1z_1,2E} P_{2E}(t) - e^{-iz_2 t} b_{1z_1,2z_2} \bar{C}_{2z_2}(t)\big]. \tag{42}$$

As in the case of the first channel, we observe that, in forming the probability $|A_{2E}(t)|^2$, the symmetric Lorentzian curve $\alpha_2^2(E)$ is modified by the spectral-asymmetry function $b_{1z_1,2E}$ of Eq. (10b) and by the time-dependent factor $P_{2E}(t)$.

The approximation by a single rectangular pulse, Eq. (20), is replaced by a summation of rectangular pulses, Eq. (28), and the integral in Eqs. (37) and (38a) is replaced by a sum of integrals,

$$\sum_{i=1}^{m} g_i \int_{t_{i-1}}^{t} dt' e^{i(E-z_2)t'} e^{iat'} C_{1z_1(i-1)}(t'), \quad t \leqslant t_m$$

For $t > t_n$, i.e., after the end of the last pulse, this function becomes a constant equal to its value at $t = t_n$.

III. SYNOPSIS OF THE FORMAL RESULTS

The formalism involves ten basic quantities. These are as follows:

(1) The energies of the ground state E_g and of the two resonances E_1 and E_2, as well as the matrix elements V_{1E_1}, V_{2E_2}, coupling the localized part of the resonance to the corresponding continuum.

(2) The dipole matrix elements d_{g1} and d_{g1E_1}, connecting the ground state to the localized part and to the continuum of the first resonance, the matrix element d_{12}, connecting the localized parts of the resonances, and d_{1E_2}, d_{2E_1}, connecting each localized part to the continuum of the other resonance.

In the calculation enter the amplitudes F_1, F_2 of the fields, and the central frequencies ω_1, ω_2. Further, the form of the envelope functions $g_1(t - t_a)$ and $g_2(t - t_b)$ must be decided on. These functions are symmetric about the times t_a and t_b respectively. The time delay is defined as $t_D = t_a - t_b$.

The external control parameters are the field strength F_2, the time delay t_D, and the duration of the pulse coupling the resonance states.

From the matrix elements mentioned above, the half widths Γ_1, Γ_2, and thus the two resonance complex poles, are computed. These poles and the frequencies of the fields provide the complex detuning parameters a_1 and a. Subsequently, the composite parameters q, Q, γ_1, γ_2 are obtained and their values are used for the calculation of the spectral-asymmetry functions b_{1E}, $b_{1E,2z_2}$, $b_{1z_1,2E}$ and of the constants b_{1z_1}, $b_{1z_1,2z_2}$ resulting from them.

A chosen shape of the envelope function, g_2, is approximated by a series of rectangular pulses. Within each rectangle, the coupling parameter $\Lambda = g_2 F_2 b_{1z_1,2z_2}$ and the complex Rabi frequency $\lambda = \sqrt{a^2 + \Lambda^2}$ are constant. The coupled differential equations (19b) and (19c)—rewritten in the compact form (A1a) and (A1b)—are solved analytically, providing the coefficients C_{1z_1} and C_{2z_2} via the formulas (27a) and (27b). The analytic solution in each rectangle is connected to that of its neighbouring rectangles by the conditions of continuity (30a) and (30b), allowing the propagation of the initial conditions in time.

The integration of Eqs. (17b) and (17c), which provides the values of the coefficients C_{1E} and C_{2E} at any energy, is subsequently done analytically within each rectangle. Finally, the coefficients and the spectral-asymmetry functions multiplying the symmetric Lorentzian distribution are combined in the formulas (36) and (42) for the photoelectron emission probability amplitudes as a function of time and energy.

The approach is transparent with respect to the parameters entering the calculation and, being analytic, with respect to the contribution made by the various parts. The formulas (27), (30), (36), and (42), used for the computation, can be easily implemented for different pulse characteristics. The results are obtained quickly and accurately.

IV. APPLICATIONS

As the first quantitative application of the present formalism for scheme (A), we calculated the time-dependent electron dynamics of the experimentally tractable scheme (B), and obtained photoelectron emission probabilities in the open channels of *both* the He $(2s2p)^1P^o$ and the He $(2p^2)^1D$ resonance states.

In order for any theoretical analysis that deals with real N-electron systems to be credible, it is crucial that the N-electron wave functions which are used for the calculation of matrix elements, i.e., of properties and phenomena, represent the corresponding states accurately, and in forms that are practical for analysis and for calculation. For example, in investigations such as the present one, the values of the quantities q and Q must be accurate. In our work, the orbitals in the configurations are obtained from the solution of the *state-specific* HF or MCHF equations. We have shown that, by starting the calculation of resonance states in this way, regardless of their electronic structure, this approach to the quantitative implementation of theories of resonance states is accurate as well as economic [30,31]. The calculation of the corresponding localized correlated wave functions and of concomitant properties of the helium DESs has been explained and justified in our work from the early 1980s, e.g., [7,32], where it was shown that determining the state-specific MCHF solutions for the ^1D resonances is feasible, in spite of the heavy configurational mixing of the configurations $2p^2$, $2p3p$, and $2s3d$. The label used here means, as usual, that the coefficient of this configuration is the largest.

The scattering orbitals for the open channels, $1s\varepsilon p$ and $1s\varepsilon d$, are calculated numerically in the potential of the ion, with energy-normalized asymptotic boundary conditions, in the fixed-core HF approximation, a procedure which eliminates intrachannel coupling.

The XUV Gaussian pulse was chosen to have the duration of 160 as, which is the one used in the experiment of [5,6]. The femtosecond pulse at $\lambda \approx 4200$ nm is coupled resonantly with the $(2p^2)$ ^1D state below, with intensities in the range 5×10^{10}–5×10^{11} W/cm^2. The lifetimes of the two resonance states are $\approx$18 fs for $(2s2p)$ $^1P^o$ and $\approx$10 fs for $(2p^2)$ ^1D.

As we already mentioned in the Introduction, the choice of the He $(2p^2)^1D$ resonance secures that the MIR femtosecond pulse does not ionize it during its coupling with the He $(2s2p)^1P^o$ state. This is because its ionization energy is about 18 times larger than the energy of the femtosecond pulse. At the same time, because the electric dipole matrix element $\langle(2s2p)^1P^o|\boldsymbol{r}|(2p^2)^1D\rangle$ is large, this choice also favors "strong" coupling even when the intensity is not very strong. Therefore, phenomena of "strong coupling," such as Rabi oscillation, are possible even at relatively low intensities such as the ones chosen here (5×10^{10}–5×10^{11} W/cm^2).

It is worth adding that such optimal choices can often be recognized ahead of calculation of the fully correlated wave functions, by considering the "Fermi-sea" zero-order wave functions and the state-specific HF orbitals only, in accordance with the concepts and methods that we have proposed and implemented over the past few decades, e.g., [31] and references therein. For example, suppose that one chose as the coupling resonance, instead of the state He $(2p^2)^1D$ (which is the lowest DES of ^1D symmetry [7]), the second ^1D DES, whose dominant configuration is the $2p3p$, and its energy is 3.34 eV above that of He $(2s2p)^1P^o$ [7]. Then, the zero-order two-electron electric dipole matrix element would be proportional to the product of the radial integrals $\langle 2s|r|2\bar{p}\rangle\langle 2p|3\bar{p}\rangle$. The very small one-electron overlap $\langle 2p|3\bar{p}\rangle$ between the nearly orthogonal $2p$ and $3\bar{p}$ orbitals reduces drastically the dipole transition amplitude. Indeed, a state-specific calculation using the correlated wave functions shows that the dipole matrix element for the transition $(2s2p)^1P^o \rightarrow (2p^2)^1D$ is about seven times larger than that for the $(2s2p)^1P^o \rightarrow (2p3p)^1D$ transition. Thus, a simple electronic structure calculation would suggest that the intensity needed to achieve strong coupling is much higher in the case of the $(2p3p)$ ^1D resonance (or of higher-lying ones) than in the optimal case of $(2p^2)^1D$. However, since the pulse coupling $(2s2p)^1P^o$ to $(2p3p)$ ^1D causes direct ionization of the latter, using high values of intensity would introduce complicating effects of higher order, theoretically as well as experimentally. Our test calculations, which we do not include for reasons of economy, support this conclusion.

The t_{FWHM} of the temporal shape of the intensity of the MIR pulse, where $t_{\mathrm{FWHM}} = 2\sqrt{\ln(2)}\sigma_b$, is chosen to be 80 fs. Since the field cycle at $\lambda \approx 4200$ nm is 14 fs, the field completes five cycles. In Fig. 3, larger values of t_{FWHM}, up to 140 fs, are used. The intensity is chosen to be 5×10^{11}W/cm^2. In Figs. 4 and 5, smaller intensity values are used, down to 5×10^{10}W/cm^2.

We define the *reduced* ionization probability densities $|A_{iE}(t)/\sigma_a F_1|^2$ derived from Eqs. (36) and (42), in order to remove the common factors with the characteristics of the first pulse, leaving the subtle dependence on the root-mean-square width of the first Gaussian pulse, σ_a, which is indicated by Eqs. (B4) and (B5) of Appendix B (see also Ref. [33]). These quantities are given in Figs. 1–5, where they are calculated at $t = 750$ fs, and in Figs. 6 and 7 for different points in time. The external control parameters are the time delay between the two pulses, the intensity, and the temporal width of the femtosecond pulse. The point $t = 750$ fs is far beyond the time necessary for the profile of the $(2s2p)^1P^o$ resonance to be complete, which is about 180 fs [3,33]. In addition, we give the time evolution of the photoelectron spectrum for specific values of the above control parameters.

In Fig. 1, the $|A_{1E}(t)/\sigma_a F_1|^2$ is shown for various time delays $t_D = t_a - t_b$ between the two pulses, where we put $t_b = 0$. t_D may range from large negative values (the short XUV pulse peaks *before* the second pulse) to large positive ones (the short XUV pulse peaks *after* the second pulse). For reasons of comparison, the result where the second pulse is absent is also shown. The results are identical in the limit of large time delays, positive or negative, in which case the second resonance state is hardly populated. The curves in the figure reflect the presence of *interference* between the two energy dependent terms of Eq. (36). At $t_D = 20$ fs, the inversion of the Fano shape, known from previous studies [12,17], is observed. As t_D increases, the resonance disappears leaving a smooth background. For still larger values of t_D, smaller population transfer occurs. Consequently, the second term is progressively diminished and the curve where the second pulse is absent is gradually reached.

In Fig. 2, the $|A_{2E}(t)/\sigma_a F_1|^2$, Eq. (42), is shown for various time delays. Two Autler-Townes peaks are observed which, for larger values of t_D, progressively merge into one at $t_D = 40$ fs. However, if the calculation is repeated for this value of t_D but with larger values of $t_{\rm FWHM}$, the two peaks reappear, as seen in Fig. 3.

This phenomenon is discussed below. In this context, we point out that a similar phenomenon of spectral recursion, having to do with the inversion of the Fano profile as a function of the laser intensity, was found and discussed by Argenti *et al.* [17] in their experimental-theoretical study of the attosecond transient absorption spectrum of helium in the energy region above 60 eV.

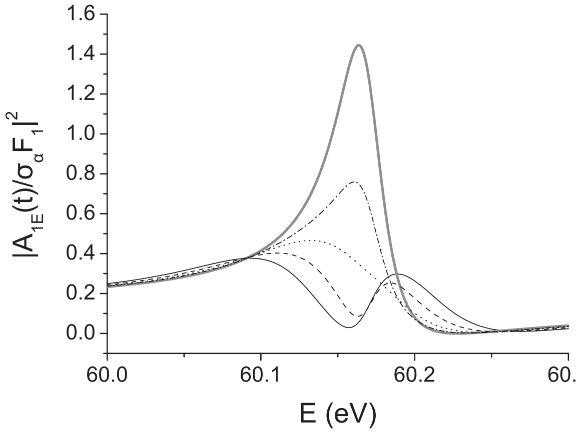

FIG. 1. Reduced ionization probability densities, calculated at long times ($t = 750$ fs), for the helium $(2s2p)^1P^o$ resonance, during the process of scheme (B), He$1s^2 \xrightarrow[60.15\text{ eV}]{160\text{ - as Gaussian pulse}} (2s2p)^1P^o \xrightarrow[0.295\text{ eV}]{\text{fs Gaussian pulse}} (2p^2)^1D$, for different values of time delay t_D. The midinfrared (MIR) Gaussian pulse has intensity $I = 5\times10^{11}\,\mathrm{W/cm^2}$ and $t_{\rm FWHM} = 80$ fs. (a) Solid line curve: $t_D = 20$ fs; (b) dashed line: $t_D = 35$ fs; (c) dotted line: $t_D = 48$ fs; (d) dash-dot: $t_D = 60$ fs; (e) thick grey line: the same quantity calculated in the absence of the second pulse. It shows the characteristic asymmetric profile of the prototypical helium $(2s2p)^1P^o$ resonance.

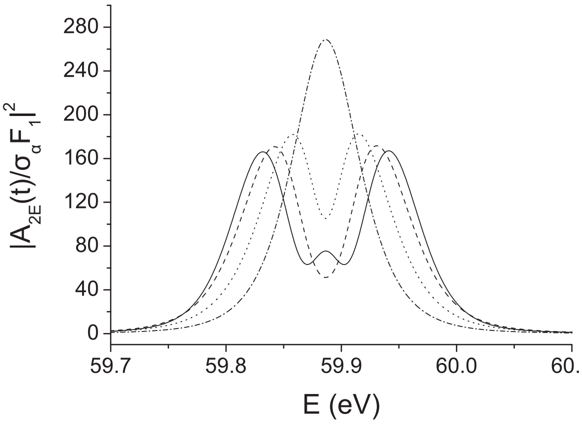

FIG. 2. Reduced ionization probability densities, calculated at long times ($t = 750$ fs), for the $(2p^2)^1D$ resonance, during the process of scheme (B), for different values of time delay t_D. The MIR Gaussian pulse has intensity $I = 5\times10^{11}\,\mathrm{W/cm^2}$ and $t_{\rm FWHM} = 80$ fs. (a) Solid line curve: $t_D = -20$ fs; (b) dashed line: $t_D = 0$ fs; (c) dotted line: $t_D = 20$ fs; (d) dash-dot: $t_D = 40$ fs. Contrary to the $(2s2p)^1P^o$ case, no signs of interference-induced asymmetry are present. Instead, the profile starts with an Autler-Townes doublet when there is enough population due to the XUV attosecond pulse excitation ($t_D = -20$ fs), and ends being symmetric for $t_D = 40$ fs.

A given width of the second pulse corresponds to a maximum number of Rabi oscillations. This number can be calculated from the expression $N_{\rm osc} = F_2 d_{12}\frac{1}{2\sqrt{2\pi\ln(2)}}t_{\rm FWHM}$, which connects $t_{\rm FWHM}$ to the number of Rabi oscillations between two *bound* states interacting resonantly via a Gaussian pulse. The formula constitutes a good approximation in the case of two resonances when Q is large. It allows one to estimate the number of Rabi oscillations that the system

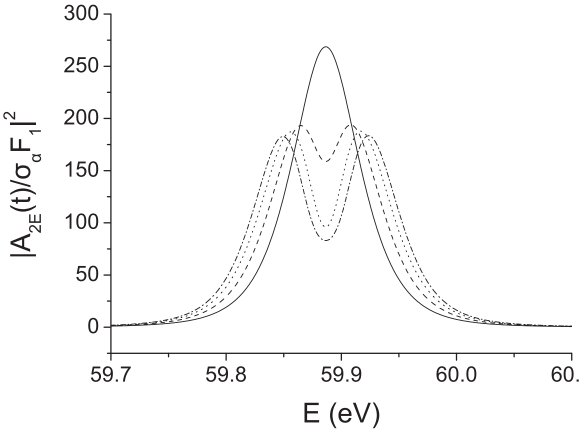

FIG. 3. Reduced ionization probability densities, calculated at long times ($t = 750$ fs), for the second channel, for the process of scheme (B), for different values of the $t_{\rm FWHM}$ of the MIR pulse. $t_D = 40$ fs and $I = 5\times10^{11}\,\mathrm{W/cm^2}$. (a) Solid line curve: $t_{\rm FWHM} = 80$ fs; (b) dashed line: $t_{\rm FWHM} = 100$ fs; (c) dotted line: $t_{\rm FWHM} = 120$ fs; (d) dash-dot: $t_{\rm FWHM} = 140$ fs. The qualitative effect of the gradual increase of the $t_{\rm FWHM}$ of the MIR pulse is the same as the one of the intensity—see Fig. 5. In both cases, the curve ends as an Autler-Townes doublet.

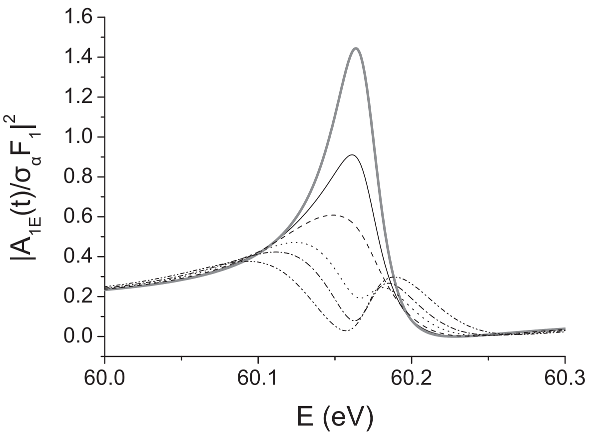

FIG. 4. Reduced ionization probability densities, calculated at long times ($t = 750$ fs), for the first channel, for the process of scheme (B), for different values of peak intensity of the MIR pulse. $t_D = 20$ fs and $t_{\rm FWHM} = 80$ fs. (a) Solid line: $I = 5\times10^{10}\,{\rm W/cm^2}$; (b) dashed line: $I = 1\times10^{11}\,{\rm W/cm^2}$; (c) dotted line: $I = 2\times10^{11}\,{\rm W/cm^2}$; (d) dash-dot line: $I = 3\times10^{11}\,{\rm W/cm^2}$; (e) dash-dot-dot line: $I = 5\times10^{11}\,{\rm W/cm^2}$; (f) thick grey line: the same quantity calculated in the absence of the second pulse. The curves show that the field-induced so-called "inversion" of the Fano profile is fully developed already at the rather low intensity of $I = 5\times10^{11}\,{\rm W/cm^2}$.

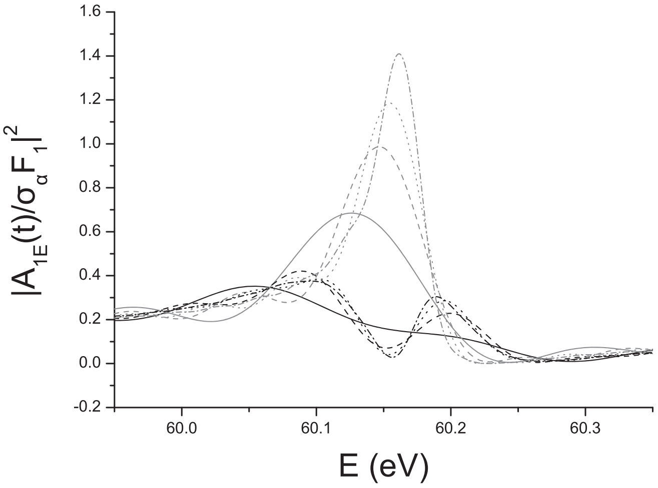

FIG. 6. Evolution of the profile of the $(2s2p)^1P^o$ resonance, for the process of scheme (B), as a function of time t. The MIR pulse has $t_{\rm FWHM} = 80$ fs and $I = 5\times10^{11}\,{\rm W/cm^2}$. $t_D = 20$ fs. (a) Black solid line: $t = 50$ fs; (b) black dashed line: $t = 70$ fs; (c) black dotted line: $t = 90$ fs; (d) black dashed-dot line: $t = 150$ fs; (e) Gray lines: The same quantity calculated in the absence of the second pulse. The curves evolve towards the corresponding ones in Fig. 1, for $t = 750$ fs.

undergoes after the ultrafast XUV pulse has acted. Actually, $N_{\rm osc}$ is reduced by the factor $\frac{1}{2}[1 - {\rm erf}(t_D/\sigma_b)]$, which for large negative time delays tends to unity while for large positive ones tends to zero. Since this factor is, in general, smaller than unity, it modifies the number of Rabi oscillations.

The above brief analysis helps to explain the behavior of $|A_{2E}(t)/\sigma_a F_1|^2$ for the larger values of t_D, where the two peaks merge into one. This behavior is due to the fact that the number of Rabi oscillations becomes smaller than 1. In Fig. 3, where the calculation is performed with the same t_D but with larger values of $t_{\rm FWHM}$, the two peaks appear again as the system is allowed to perform at least one Rabi cycle.

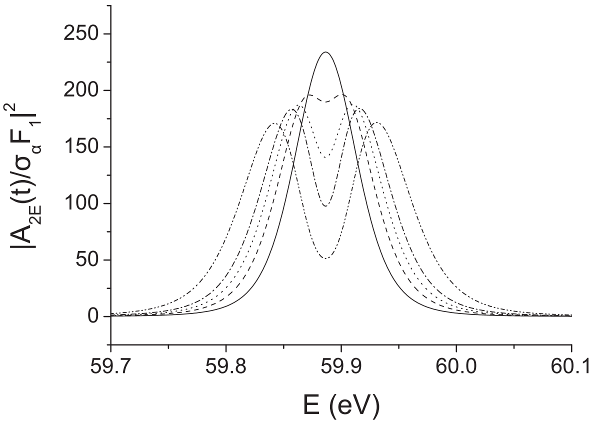

FIG. 5. Reduced ionization probability densities, calculated at long times ($t = 750$ fs), for the second channel, for the process of scheme (B), for different values of peak intensity of the MIR pulse. $t_D = 0$ fs and $t_{\rm FWHM} = 80$ fs. (a) Solid line: $I = 1\times10^{11}\,{\rm W/cm^2}$; (b) dashed line: $I = 1.7\times10^{11}\,{\rm W/cm^2}$; (c) dotted line: $I = 2.3\times10^{11}\,{\rm W/cm^2}$; (d) dash-dot line: $I = 3\times10^{11}\,{\rm W/cm^2}$; (e) dash-dot-dot line: $I = 5\times10^{11}\,{\rm W/cm^2}$.

In conclusion, in addition to the intensity, the width of the second pulse is a crucial parameter for the control of the photoelectron emission probability in the discrete-resonance-resonance transitions, for a given value of time delay.

In contradistinction to Figs. 2 and 3, Fig. 1 shows no Autler-Townes splitting. This is because the lifetime of $(2p^2)\ ^1D$ is only ≈10 fs, i.e., smaller than that of the $(2s2p)\ ^1P^o$ resonance (≈18 fs), resulting in a small transfer of population to the first channel. Note that, as mentioned above, the observed structure is the result of *interference* between the energy dependent terms of Eq. (36).

Figures 4 and 5 show the findings for the effect of the peak intensity of the MIR pulse on the photoelectron spectra of the first and the second channel respectively, for fixed values of the time delay. The chosen values are, $t_D = 20$ fs for the first channel, where the intensity is gradually reduced down to $5\times10^{10}\,{\rm W/cm^2}$, and $t_D = 0$ fs for the second channel, where the intensity is gradually reduced down to $10^{11}\,{\rm W/cm^2}$. In Fig. 4, the decrease of the intensity results in a photoelectron spectrum which gradually approaches the spectrum that is formed when the second pulse is absent. In Fig. 5, the effect of the decrease of the intensity is the disappearance of the Autler-Townes splitting, as the number of Rabi oscillations becomes smaller than 1.

In Fig. 6, the quantity $|A_{1E}(t)/\sigma_a F_1|^2$ is given as a function of time t for a fixed value of time delay. This value is $t_D = 20$ fs, for which, as seen from Fig. 1, the inversion of the Fano shape has taken place. For reasons of comparison, we include the same quantity calculated in the absence of the second pulse. This curve evolves towards the one in Fig. 1, where it is given for $t = 750$ fs.

Finally, Fig. 7 depicts the time-dependent formation of the $(2p^2)\ ^1D$ resonance. The quantity $|A_{2E}(t)/\sigma_a F_1|^2$ is given as

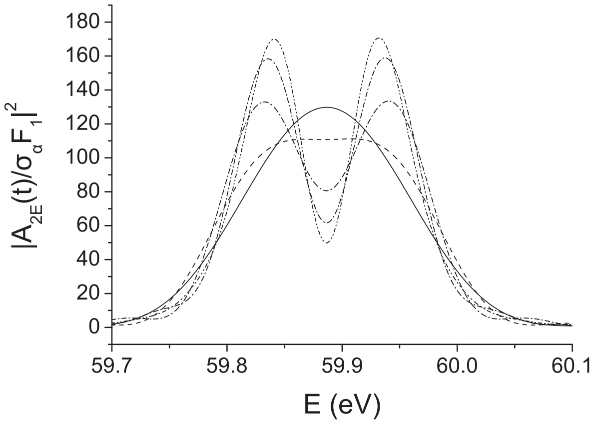

FIG. 7. Time evolution of the profile of the $(2p^2)^1D$ resonance, for the process of scheme (B). The MIR pulse has $t_{\mathrm{FWHM}} = 80$ fs and $I = 5{\times}10^{11}\,\mathrm{W/cm^2}$. $t_D = 20$ fs. (a) Solid line: $t = 30$ fs; (b) dashed line: $t = 40$ fs; (c) dotted line: $t = 50$ fs; (d) dashed-dot line: $t = 60$ fs; (e) dashed-dot-dot line: $t = 80$ fs. The curve evolves toward the corresponding one in Fig. 2 for $t = 750$ fs.

a function of t for a fixed value of time delay, $t_D = 0$ fs. The profile starts as a broad line, whose width diminishes as time increases until it is split in two Autler-Townes peaks. Note that as time evolves, the peak does not acquire any asymmetry due to interference, as is the case with the $(2s2p)\ ^1P^o$ resonance. This result is due to the fact that the value of Q is very large (≈ -1300). (See the results and discussion of Sec. II B.)

V. CONCLUSION

The theory of this paper first solved analytically the TD3L problem described by scheme (A), for the case where the second pulse has a rectangular temporal shape. Based on this result, we solved this TD3L problem for any shape of the two pulses, including a Gaussian one. Assuming excitation by an attosecond pulse, the second pulse can have any central frequency and any moderately strong-field strength that is physically acceptable for each system of interest.

In principle, the METDSE describing the interaction of an N-electron atomic state with two-color attosecond-femtosecond pulses reaching resonance states in the continuum and applied with positive, zero, or negative time delay t_D can be solved numerically for arbitrary electronic structures via the *state-specific expansion approach* (SSEA), e.g., [24]. However, since this endeavor is computationally demanding, it is desirable to be able to tackle certain interesting problems, such as the TD2L [3,33] or the present TD3L (scheme A), in terms of analytic models that provide accurate solutions under physically appropriate conditions. The availability of such analytic expressions reduces by orders of magnitude the size of the computation, especially because the contribution of the scattering continuum, which in the case of the SSEA is computed by including in the expansion of $\Psi(t)$ thousands of numerically calculated state-specific energy-normalized scattering wave functions, is now included in terms of properly defined calculable analytic expressions.

Central to our approach is the expansion in eigenfunctions, so that the field-free Hamiltonian is diagonal within each angular momentum subspace. This is in contrast to the expansion in terms of the localized and scattering components used in the literature for the solution of this three-level problem. In the latter case, the coefficients of the scattering components are initially decoupled through an additional assumption, as mentioned in the Introduction. In contradistinction, the eigenstate expansion permits a neat way of dealing with the continuum of scattering states without any approximation. Thus, one is led to the simplicity of Eqs. (17) where the coefficients of the eigenstates depend solely upon their values at the complex energy poles. To solve the resulting intermediate equations (19) we chose an approach leading to semianalytic results which can be evaluated in a couple of seconds once the necessary wave functions and matrix elements have been computed.

As summarized in Sec. III, the final analytic formulas involve calculable N-electron matrix elements. Of course, the accurate calculation of these matrix elements is a crucial desideratum for reliable numerical predictions. In our work, the corresponding wave functions for the discrete and for the resonance wave functions are calculated according to the *state- and property-specific* theory, e.g., [30,31]. In this first application, we dealt with the calculation of the photoelectron emission probabilities for the case

$$\mathrm{He}1s^2 \xrightarrow[60.15\,\mathrm{eV}]{160\text{ - as Gaussian pulse}} (2s2p)^1P^o \xrightarrow[0.295\,\mathrm{eV}]{\text{fs Gaussian pulse}} (2p^2)^1D.$$

Emission probabilities in both channels were studied, for various times, thereby determining the time-resolved formation not only of the first resonance, $(2s2p)\ ^1P^o$, but also of the second one. As control parameters we used the intensity, the temporal width of the femtosecond pulse, and the time delay (Figs. 1–7).

APPENDIX A

We solve the system of equations,

$$\dot{C}_{1z_1}(t) = \tfrac{1}{2}e^{i\varphi_1}F_1 g_1(t)\, b_{1z_1} e^{ia_1 t} - \tfrac{1}{2}e^{-i\varphi_2}\Lambda e^{-iat} C_{2z_2}(t), \tag{A1a}$$

$$\dot{C}_{2z_2}(t) = \tfrac{1}{2}e^{i\varphi_2}\Lambda e^{iat} C_{1z_1}(t). \tag{A1b}$$

This is an inhomogeneous system of linear differential equations for the coefficients of the localized components of the two resonances. The exponential factors are removed from the second term of (A1a) and from (A1b) by the transformation

$$C_{1z_1}(t) = B_{1z_1}(t)e^{-iat/2}, \tag{A2a}$$

$$C_{2z_2}(t) = B_{2z_2}(t)e^{iat/2}. \tag{A2b}$$

The new dependent variables satisfy the equations

$$\dot{B}_{1z_1}(t) - i\tfrac{1}{2}aB_{1z_1}(t) = \tfrac{1}{2}e^{i\varphi_1}F_1 e^{-i(\varepsilon-a)t/2}e^{ia_1 t} g_1(t)\, b_{1z_1} - \tfrac{1}{2}e^{-i\varphi_2}\Lambda B_{2z_2}(t), \tag{A3a}$$

$$\dot{B}_{2z_2}(t) + i\tfrac{1}{2}aB_{2z_2}(t) = \tfrac{1}{2}e^{i\varphi_2}\Lambda B_{1z_1}(t). \tag{A3b}$$

By excluding the inhomogeneous term, (A3) becomes a time-independent homogeneous system which is solved as a complex eigenvalue problem with eigenvalues $\varepsilon = \pm\lambda$ where λ is the complex Rabi frequency. Thus, the general solution of the homogeneous system is a linear combination of the two eigenvectors with coefficients determined from the boundary conditions at $t = t_0$. The general solution of the nonhomogeneous system is subsequently obtained by adding the solution of the homogeneous system to a particular solution of the inhomogeneous one according to a standard procedure (see below). Finally, after the $B_{1z_1}(t)$ and $B_{2z_2}(t)$ coefficients are determined, they are multiplied by $e^{-iat/2}$ and $e^{iat/2}$ respectively to give $C_{1z_1}(t)$ and $C_{2z_2}(t)$.

The *homogeneous* system resulting from that of Eqs. (A3) is of the form $\dot{\underline{x}} = \frac{i}{2}A\underline{x}$. Its solution is found by putting $\underline{x}(t) = \underline{x}_0 e^{i\varepsilon t/2}$ and by solving the resulting eigenvalue problem $A\underline{x}_0 = \varepsilon\underline{x}_0$. In our case,

$$A = \begin{pmatrix} a & i\Lambda e^{-i\varphi_2} \\ -i\Lambda e^{i\varphi_2} & -a \end{pmatrix}. \tag{A4}$$

We find the eigenvalues $\varepsilon = \pm\lambda$ and (un-normalized) eigenvectors $\underline{x}_0^{\pm}$ where

$$\lambda \equiv \sqrt{a^2 + \Lambda^2} \tag{A5}$$

and

$$\underline{x}_0^{+} = \frac{1}{2\lambda}\begin{pmatrix} \lambda + a \\ -i\Lambda e^{i\varphi_2} \end{pmatrix}, \quad \underline{x}_0^{-} = \frac{1}{2\lambda}\begin{pmatrix} \lambda - a \\ i\Lambda e^{i\varphi_2} \end{pmatrix}. \tag{A6}$$

The general solution of the homogeneous system is $\underline{x}(t) = c_+\underline{x}_0^{+}e^{i\lambda t/2} + c_-\underline{x}_0^{-}e^{-i\lambda t/2}$.

The system of Eqs. (A3) is a nonhomogeneous system of the form $\dot{\underline{x}} = A\underline{x} + \underline{f}$. Its general solution consists of the general solution of the homogeneous system plus a particular solution of the inhomogeneous one. The latter is found by the following procedure: The matrix A is diagonalized by the similarity transformation $T^{-1}AT = A_d$ where the matrix T contains in its columns the eigenvectors $\underline{x}_0^{\pm}$ and the diagonal matrix A_d contains the eigenvalues $\pm\lambda$. Thus, the inhomogeneous system can be written as $\dot{\underline{x}} = TA_dT^{-1}\underline{x} + \underline{f}$ and putting $\underline{y} = T^{-1}\underline{x}$ and $\underline{h} = T^{-1}\underline{f}$ we obtain the equivalent system $\dot{\underline{y}} = A_d\underline{y} + \underline{h}$. Since A_d is a diagonal matrix, the equations of the equivalent system are decoupled and can be solved by standard methods. The solution has the form

$$y_{\pm} = c_{\pm}e^{\pm i\lambda t/2} + e^{\pm i\lambda t/2}\int_{t_0}^{t} dt' e^{\mp i\lambda t'/2}h_{\pm}(t'). \tag{A7}$$

When multiplied by T, the first term produces the general solution of the homogeneous system, while the second term produces a particular solution of the inhomogeneous one. In what follows we shall focus on the latter.

Define the integral operators

$$K_{\pm}\phi \equiv e^{\pm i\lambda t/2}\int_{t_0}^{t} dt' e^{\mp i\lambda t'/2}\phi(t'), \tag{A8}$$

operating on a test function ϕ and, through them, the diagonal matrix K_d with matrix elements calculated through $K_{\pm}$. The particular solution of the inhomogeneous system is now written as $\underline{y} = K_d\underline{h}$, giving, after the back transformation, $\underline{x} = TK_dT^{-1}\underline{f}$. Note that the second component of $\underline{f}$ is zero since Eq. (A1b) has no inhomogeneous term. This procedure leads to Eqs. (27) of the main text.

APPENDIX B

The integrals $G^{(2)}(\zeta, t)$ of Eq. (32a) are evaluated through integration by parts with the result

$$\begin{aligned} G^{(2)}(\zeta, w, t) &\equiv \int_{t_0}^{t} dt' e^{i\zeta t'}[c + G^{(1)}(w, t')] \\ &= \frac{1}{i\zeta}e^{i\zeta t}[c + G^{(1)}(w, t)] - \frac{1}{i\zeta}e^{i\zeta t_0}c \\ &\quad - \frac{1}{i\zeta}\int_{t_0}^{t} dt' e^{i(w+\zeta)t'}g_1(t'). \end{aligned} \tag{B1}$$

The integral in the third term of (B1) is equal to $G^{(1)}(w + \zeta, t)$ therefore

$$\begin{aligned} G^{(2)}(\zeta, w, t) &= -i\frac{1}{\zeta}e^{i\zeta t}[c + G^{(1)}(w, t)] \\ &\quad + i\frac{1}{\zeta}e^{i\zeta t_0}c + i\frac{1}{\zeta}G^{(1)}(w + \zeta, t). \end{aligned} \tag{B2}$$

The same result applies for $G^{(2)}(\xi, w, t)$ of Eq. (40a).

In the case where the envelope function is a Gaussian, i.e., $g_1(t) = e^{-(t-t_a)^2/2\sigma_a^2}$, the integrals $G^{(1)}(w, t)$ of Eq. (29a) are expressed in terms of the *error function* defined as

$$\int_0^t dt' e^{-c^2t'^2} = \frac{\sqrt{\pi}}{2c}\text{erf}(ct). \tag{B3}$$

From the basic integral (B3) one easily obtains

$$\begin{aligned} G^{(1)}(w, t) &\equiv \int_{t_0}^{t} dt' e^{-c^2(t'-t_a)^2 + iwt'} \\ &= \frac{\sqrt{\pi}}{2c}e^{iw[t_a-(1/2)t_w]}\{\text{erf}[c(t - t_a + t_w)] \\ &\quad - \text{erf}[c(t_0 - t_a + t_w)]\}, \end{aligned} \tag{B4}$$

where

$$t_w = -iw/2c^2. \tag{B5}$$

In the above formulas, $c = \frac{1}{\sigma_a\sqrt{2}}$. Consequently, $\text{Re}t_w = \sigma_a^2\text{Im}w$ and the real part of time t_w, although expected to be small from Eq. (27b), can have a significant value in the case of a broad Gaussian.

APPENDIX C

In this appendix a Gaussian pulse $e^{-(t-t_b)^2/2\sigma^2}$, centered at t_b and having root-mean-square width σ, is approximated by a sum of n rectangular pulses as

$$g_2(t) \approx \sum_{i=1}^{n} g_i[St(t - t_{i-1}) - St(t - t_i)] \tag{C1}$$

in a series of successive approximations. We start with a single rectangle

$$g_2(t) \approx St(t - t_0) - St(t - t_1), \tag{C2}$$

where $t_0 = t_b - p\sigma$, $t_1 = t_b + p\sigma$, i.e., a pulse of duration $\delta = 2p\sigma$ centered at t_b and p is a positive number. We require the presence, at each level of approximation, of a central rectangle of height equal to 1 as in (C2) from whose center the time delay will be calculated.

Each successive level of approximation consists of a number of pulses $n_k = 2n_{k-1} + 1$ of duration $\delta_k = \frac{1}{2}\delta_{k-1}$ where n_{k-1} and δ_{k-1} are the corresponding values at the previous level, the first one being the single rectangle. Consequently, $n_k = 2^k - 1$ and $\delta_k = \frac{1}{2^{k-1}} 2p\sigma$ for $k \geqslant 1$. Thus, the rectangles of the kth approximation have their widths subdivided compared to those of the $(k-1)$th while the new rectangles appear between the positions of the old ones.

The interval of the central pulse in the kth approximation is $[t_b - \frac{1}{2^{k-1}} p\sigma,\ t_b + \frac{1}{2^{k-1}} p\sigma]$ while the first rectangular pulse starts at $t_0 = t_b - n_k\delta_k/2$. The centers of the n_k intervals at the kth level of approximation for $k > 1$ occur, besides t_b, at n_{k-1}*pairs* of points about t_b specifically at $t_b \pm m\delta_k$, $1 < m \leqslant n_{k-1}$. The heights of the Gaussian at these points provide the values of the weights g_i.

For large values of k we obtain $t_0 \to t_b - 2p\sigma$. Thus the Gaussian is approximated in the interval $[t_b - 2p\sigma\ ,\ t_b + 2p\sigma]$ at the end points of which it has fallen at e^{-2p^2} of its height. This procedure can be applied for any pulse shape which is symmetric about t_b.

[1] C. A. Nicolaides, Th. Mercouris, and Y. Komninos, Attosecond dynamics of electron correlation in doubly excited atomic states, J. Phys. B: At. Mol. Opt. Phys. **35**, L271 (2002).

[2] Th. Mercouris, Y. Komninos, and C. A. Nicolaides, Theory and computation of the attosecond dynamics of pairs of electrons excited by high-frequency short light pulses, Phys. Rev. A **69**, 032502 (2004).

[3] Th. Mercouris, Y. Komninos, and C. A. Nicolaides, Time-dependent formation of the profile of the He $2s2p\,^1P^o$ state excited by a short laser pulse, Phys. Rev. A **75**, 013407 (2007); **87**, 069905(E) (2013).

[4] Th. Mercouris, Y. Komninos, and C. A. Nicolaides, Time-resolved hyperfast processes of strongly correlated electrons during the coherent excitation and decay of multiply excited and inner-hole states, Phys. Rev. A **76**, 033417 (2007).

[5] A. Kaldun, A. Blättermann, V. Stooß, S. Donsa, H. Wei, R. Pazourek, S. Nagele, C. Ott, C. D. Lin, J. Burgdörfer, and T. Pfeifer, Observing the ultrafast buildup of a Fano resonance in the time domain, Science **354**, 738 (2016).

[6] A. Blättermann, A. Kaldun, V. Stooß, S. Donsa, H. Wei, R. Pazourek, S. Nagele, C. Ott, C. D. Lin, J. Burgdörfer, and T. Pfeifer, Watching the emergence of a Fano resonance in doubly excited helium, J. Phys.: Conf. Ser. **875**, 012010 (2017).

[7] G. Aspromallis, Y. Komninos, and C. A. Nicolaides, Electron correlation and relativistic effects on the energies and widths of doubly excited states of He, J. Phys. B: At. Mol. Phys. **17**, L151 (1984).

[8] Z.-H. Loh, C. H. Greene, and S. R. Leone, Femtosecond induced transparency and absorption in the extreme ultraviolet by coherent coupling of the He $2s2p\,^1P^o$ and $2p^2\ ^1S^e$ double excitation states with 800 nm light, Chem. Phys. **350**, 7 (2008).

[9] S. Gilbertson, M. Chini, X. Feng, S. Khan, Y. Wu, and Z. Chang, Monitoring and Controlling the Electron Dynamics in Helium with Isolated Attosecond Pulses, Phys. Rev. Lett. **105**, 263003 (2010).

[10] W.-C. Chu, S.-F. Zhao, and C. D. Lin, Laser-assisted-autoionization dynamics of helium resonances with single attosecond pulses, Phys. Rev. A **84**, 033426 (2011); W.-C. Chu and C. D. Lin, Theory of ultrafast autoionization dynamics of Fano resonances, *ibid.* **82**, 053415 (2010).

[11] W.-C. Chu and C. D. Lin, Photoabsorption of attosecond XUV light pulses by two strongly laser-coupled autoionizing states, Phys. Rev. A **85**, 013409 (2012).

[12] W.-C. Chu and C. D. Lin, Absorption and emission of single attosecond light pulses in an autoionizing gaseous medium dressed by a time-delayed control field, Phys. Rev. A **87**, 013415 (2013).

[13] M. Tarana and C. H. Greene, Femtosecond transparency in the extreme-ultraviolet region, Phys. Rev. A **85**, 013411 (2012).

[14] C. Ott, A. Kaldun, P. Raith, K. Meyer, M. Laux, J. Evers, C. H. Keitel, C. H. Greene, and T. Pfeifer, Lorentz meets Fano in spectral line shapes: A universal phase and its laser control, Science **340**, 716 (2013).

[15] C. Ott, A. Kaldun, L. Argenti, P. Raith, K. Meyer, M. Laux, Y. Zhang, A. Blättermann, S. Hagstotz, T. Ding, R. Heck, J. Madroñero, F. Martín, and T. Pfeifer, Reconstruction and control of a time-dependent two-electron wave packet, Nature (London) **516**, 374 (2014).

[16] Z. Q. Yang, D. F. Ye, T. Ding, T. Pfeifer, and L. B. Fu, Attosecond XUV absorption spectroscopy of doubly excited states in helium atoms dressed by a time-delayed femtosecond infrared laser, Phys. Rev. A **91**, 013414 (2015).

[17] L. Argenti, A. Jiménez-Galán, C. Marante, C. Ott, T. Pfeifer, and F. Martín, Dressing effects in the attosecond transient absorption spectra of doubly excited states in helium, Phys. Rev. A **91**, 061403(R) (2015).

[18] L. Madsen, P. Schlaghek, and P. Lambropoulos, Laser-induced transitions between triply excited hollow states, Phys. Rev. A **62**, 062719 (2000).

[19] H. Bachau, P. Lambropoulos, and R. Shakeshaft, Theory of laser-induced transitions between autoionizing states of He, Phys. Rev. A **34**, 4785 (1986).

[20] N. E. Karapanagioti, D. Charalambidis, C. J. G. J. Uiterwaal, C. Fotakis, H. Bachau, I. Sanchez, and E. Cormier, Effects of coherent coupling of autoionizing states on multiphoton ionization, Phys. Rev. A **53**, 2587 (1996).

[21] Th. Mercouris and C. A. Nicolaides, Computation of the widths of doubly excited states coupled by external AC or DC fields, J. Phys. B: At. Mol. Opt. Phys. **24**, L557 (1991).

[22] C. A. Nicolaides and S. I. Themelis, Doubly excited autoionizing states in a DC field. Widths, polarizabilities and hyperpolarizabilities of the He $2s^2\ ^1S$ and $2s2p\,^3P^o$ states, J. Phys. B: At. Mol. Opt. Phys. **26**, L387 (1993).

[23] M. Bylicki, S. I. Themelis, and C. A. Nicolaides, State-specific theory and computation of a polyelectronic atomic state in a

magnetic field. Application to doubly excited states of H^-, J. Phys. B: At. Mol. Opt. Phys. **27**, 2741 (1994).

[24] Th. Mercouris, Y. Komninos, and C. A. Nicolaides, The state-specific expansion approach to the solution of the polyelectronic time-dependent Schrödinger equation for atoms and molecules in unstable states, Adv. Quantum Chem. **60**, 333 (2010).

[25] Y. Komninos, Th. Mercouris, and C. A. Nicolaides, Theory and computation of electromagnetic transition matrix elements in the continuous spectrum of atoms, Eur. Phys. J. D **71**, 8 (2017).

[26] U. Fano, Effect of configuration interaction on intensities and phase shifts, Phys. Rev. **124**, 1866 (1961).

[27] Y. Komninos and C. A. Nicolaides, Theory and computation of the profile of the free–free transition probability between autoionizing (resonant) states, J. Phys. B: At. Mol. Opt. Phys. **30**, L237 (1997).

[28] Y. Komninos and C. A. Nicolaides, Effects of configuration interaction on photoabsorption spectra in the continuum, Phys. Rev. A **70**, 042507 (2004).

[29] U. Eichmann, T. F. Gallagher, and R. M. Konik, Fano Line Shapes Reconsidered: Symmetric Photoionization Peaks from Pure Continuum Excitation, Phys. Rev. Lett. **90**, 233004 (2003); **94**, 229302 (2005); J. W. Cooper, C. H. Greene, P. W. Langhoff, A. F. Starace, and C. Winstead, Comment on "Fano Line Shapes Reconsidered: Symmetric Photoionization Peaks from Pure Continuum Excitation", *ibid.* **94**, 229301 (2005).

[30] C. A. Nicolaides, Theory and state-specific methods for the analysis and computation of field-free and field-induced unstable states in atoms and molecules, Adv. Quantum Chem. **60**, 163 (2010).

[31] C. A. Nicolaides, Resonances in the continuum, field-induced nonstationary states, and the state- and property-specific treatment of the many-electron problem, Adv. Quantum Chem. **74**, 149 (2017).

[32] Y. Komninos, N. Makri, and C. A. Nicolaides, Electronic structure and the mechanism of autoionization for doubly excited states, Z. Phys. D **2**, 105 (1986).

[33] C. A. Nicolaides, Th. Mercouris, and Y. Komninos, Time-dependent formation of the profile of resonance atomic states and its dependence on the duration of ultrashort pulses from free-electron lasers, Phys. Rev. A **80**, 055402 (2009).